Research Square

Preprints are preliminary reports that have not undergone peer review.
They should not be considered conclusive, used to inform clinical practice,
or referenced by the media as validated information.

RCC2 functions as a spatial scaffold bridging EPHA3 and YBX1 to drive gastric cancer metastasis via ITGB1 transcription

Jingli Xu

joinleo03@163.com

Zhejiang Cancer Hospital https://orcid.org/0000-0003-2469-4628

Qianyu Zhao
Ruolan Zhang
Chunyan Weng
Qi Li
Jingjing Wang
Zhiqin Wang
Chunlian Zhai
Ziyang Huang
Xiongyang Yang
Yangyang Zhang
Can Hu
Zhiyuan Xu
Zhejiang Cancer Hospital

Article

Keywords: RCC2, gastric cancer, metastasis, YBX1, ITGB1, EPHA3

Posted Date: June 10th, 2026

DOI: https://doi.org/10.21203/rs.3.rs-9919908/v1

License: This work is licensed under a Creative Commons Attribution 4.0 International License.
Read Full License

Additional Declarations: There is **NO** conflict of interest to disclose.

RCC2 functions as a spatial scaffold bridging EPHA3 and YBX1 to drive gastric cancer metastasis via ITGB1 transcription

Qianyu Zhao[1,2,#], Ruolan Zhang[1,3,#], Chunyan Weng[3,#], Qi Li[1], Jingjing Wang[1], Zhiqin Wang[1], Chunlian Zhai[1], Ziyang Huang[1], Xiongyang Yang[1], Yangyang Zhang[1], Can Hu[1,2,*], Zhiyuan Xu[1,2,*], Jingli Xu[1,2,*]

[1]Department of Gastric Surgery, Zhejiang Cancer Hospital, Hangzhou Institute of Medicine (HIM), Chinese Academy of Sciences, Hangzhou, Zhejiang 310022, China

[2]Zhejiang Provincial Research Center for Upper Gastrointestinal Tract Cancer, Zhejiang Cancer Hospital, Hangzhou 310022, China.

[3]The first affiliated hospital of Zhejiang Chinese Medical University, Hangzhou, Zhejiang 310053, China

[#]These authors contributed equally.

*Correspondence to:

Jingli Xu, Department of Gastric Surgery, Zhejiang Cancer Hospital, Hangzhou Institute of Medicine (HIM), Chinese Academy of Sciences, Hangzhou, Zhejiang 310022, China, joinleo03@163.com.

Zhiyuan Xu, Department of Gastric Surgery, Zhejiang Cancer Hospital, Hangzhou Institute of Medicine (HIM), Chinese Academy of Sciences, Hangzhou, Zhejiang 310022, China, xuzy@zjcc.org.cn.

Can Hu, Department of Gastric Surgery, Zhejiang Cancer Hospital, Hangzhou Institute of Medicine (HIM), Chinese Academy of Sciences, Hangzhou, Zhejiang 310022, China, hucan@zjcc.org.cn.

Abstract

Regulator of chromosome condensation 2 (RCC2) has been implicated in cancer progression, yet its functional role and molecular mechanism in gastric cancer (GC) remain unclear. Here, we report that RCC2 is markedly upregulated in GC tissues and is associated with tumor metastasis and unfavorable prognosis. Analyses of TCGA datasets and single-cell RNA sequencing of primary tumors, adjacent non-tumor tissues, and metastatic lesions revealed a metastasis-associated increase of RCC2, particularly in malignant epithelial cells. Functional studies demonstrated that RCC2 knockdown suppressed GC cell proliferation, migration, and invasion in vitro, and significantly inhibited tumor growth and dissemination in subcutaneous, orthotopic, and peritoneal metastasis models. Quantitative proteomic analysis identified integrin beta 1 (ITGB1) as a key downstream effector of RCC2, and restoration of ITGB1 expression reversed the inhibitory effects of RCC2 depletion on GC progression both in vitro and in vivo. Mechanistically, RCC2 regulated ITGB1 transcription by promoting nuclear localization of the transcription factor Y-box binding protein 1 (YBX1). Notably, we identified that RCC2 functions as an indispensable scaffold protein that physically bridges the receptor tyrosine kinase EPHA3 and YBX1. This ternary complex assembly facilitates EPHA3-mediated YBX1 phosphorylation at the Y162 residue, which was required for YBX1 nuclear translocation and transcriptional activation of ITGB1. Together, these findings uncover a previously unrecognized EPHA3–RCC2–YBX1–ITGB1 axis that drives gastric cancer progression and metastasis, highlighting this scaffold-dependent signaling network as a potential therapeutic target.

Key words: RCC2; gastric cancer; metastasis; YBX1; ITGB1; EPHA3

1. Introduction

Gastric cancer (GC) remains one of the most common malignancies and a leading cause of cancer-related mortality worldwide[1]. Despite advances in early detection and multimodal treatment strategies, the prognosis of patients with advanced GC remains

dismal, largely due to aggressive invasion, distant metastasis, and frequent recurrence[2]. In particular, peritoneal dissemination represents a predominant and lethal metastatic pattern in GC, often accompanied by malignant ascites and intestinal obstruction, which severely compromise patient survival and quality of life[3]. Elucidating the molecular mechanisms that drive GC metastasis is therefore critical for the development of effective therapeutic strategies.

Metastatic progression is a complex, multistep process requiring the coordinated regulation of cell proliferation, migration, adhesion, and interaction with the extracellular matrix[4]. Integrin-mediated signaling plays a central role in these processes by transmitting mechanical and biochemical cues from the tumor microenvironment to intracellular signaling pathways[5]. Aberrant activation of integrin pathways has been widely implicated in tumor invasion and metastatic dissemination[6]; however, the upstream regulatory mechanisms governing integrin signaling in GC remain incompletely understood.

Regulator of chromosome condensation 2 (RCC2), also known as TD-60, was initially identified as a mitosis-associated protein involved in telophase disc formation and chromosome segregation[7]. Subsequent studies revealed that RCC2 functions as a guanine nucleotide exchange factor (GEF) for the small GTPase RalA and is essential for proper mitotic progression, spindle assembly, and cytokinesis, thereby maintaining genomic stability[8 9 10]. Beyond its canonical roles in cell division, emerging evidence indicates that RCC2 also participates in the regulation of cell motility, suggesting a potential role in cancer progression [11].

Indeed, accumulating studies have reported aberrant RCC2 expression across multiple human malignancies, where it has been linked to enhanced tumor growth, metastatic behavior, unfavorable prognosis, and therapeutic resistance[12]. For example, RCC2 has been shown to promote estrogen receptor–positive breast cancer progression by enhancing migratory capacity and suppressing apoptosis, while in lung adenocarcinoma, elevated RCC2 expression facilitates metastatic dissemination through activation of MAPK–JNK signaling and induction of epithelial–mesenchymal transition[13]. In gastric cancer, our previous work demonstrated that reactive oxygen

species–induced ubiquitination and degradation of RCC2 critically regulate peritoneal metastasis, and that inhibition of GPX4 can trigger RCC2 ubiquitination[14]. However, despite these observations, the downstream effectors and the precise molecular mechanisms through which RCC2 drives GC progression and metastasis remain largely undefined.

In this study, we systematically investigated the expression pattern, biological function, and mechanistic role of RCC2 in gastric cancer. By integrating bulk and single-cell transcriptomic analyses, quantitative proteomics, and comprehensive functional assays in vitro and in vivo, we identified a previously unrecognized EPHA3–RCC2–YBX1–ITGB1 signaling axis that promotes GC growth and metastatic dissemination. Mechanistically, we discovered that RCC2 functions as a crucial spatial scaffold that physically bridges the receptor tyrosine kinase EPHA3 and the transcription factor YBX1. This structural assembly facilitates EPHA3-mediated phosphorylation of YBX1 at the Y162 residue, driving its nuclear translocation and subsequent transcriptional activation of ITGB1, thereby amplifying integrin–FAK signaling. These findings uncover a novel structural and regulatory mechanism underlying GC progression and highlight this scaffold-dependent signaling network as a highly promising therapeutic target for advanced and metastatic gastric cancer.

Materials and Methods

TCGA data acquisition and bioinformatic analyses

RNA sequencing data processed by the STAR pipeline for 33 tumor types were downloaded from the Genomic Data Commons (GDC) portal (https://portal.gdc.cancer.gov). Transcript abundance was quantified as transcripts per million (TPM). Pan-cancer analysis was performed to compare RCC2 expression between tumor tissues and corresponding adjacent normal tissues. For gastric cancer–specific analyses, TCGA-STAD datasets were curated, and paired tumor and adjacent non-tumor samples were analyzed. Correlation analysis between RCC2 and ITGB1 expression was performed using TCGA-STAD data. Survival analyses, including overall survival (OS) and first progression (FP), were conducted using the Kaplan–

Meier Plotter database, with patients stratified according to RCC2 expression levels.

Patient samples and ethical approval

Gastric cancer tissues, matched adjacent non-tumor tissues, and metastatic lesions were collected from patients who underwent surgical resection at Zhejiang Cancer Hospital. A total of 93 gastric cancer patients were enrolled, yielding 141 samples for downstream analyses. These samples comprised 18 adjacent non-tumor tissues (adja), 61 primary gastric cancer tissues without metastasis (pri_nm), 16 primary gastric cancer tissues with metastasis (pri_m), 10 liver metastases (liver), 11 ovarian metastases (ovary), 14 peritoneal metastases (peritoneal), and 11 ascites samples (ascites). None of the patients received chemotherapy or radiotherapy prior to surgery. All tissue samples were obtained with written informed consent from the patients. The study protocol was approved by the Ethics Committee of Zhejiang Cancer Hospital (approval number: IRB-2023-960(IIT)) and was conducted in accordance with the Declaration of Helsinki.

For protein validation, five paired gastric cancer tissues and matched adjacent non-tumor tissues were freshly collected, immediately snap-frozen in liquid nitrogen, and stored at −80 °C until use.

Single-cell RNA sequencing analysis

Single-cell RNA sequencing (scRNA-seq) was performed on primary gastric cancer tissues, matched adjacent non-tumor tissues, and corresponding metastatic lesions collected at Zhejiang Cancer Hospital. Single-cell suspensions were prepared using standard protocols. Downstream data processing, including quality control, normalization, dimensionality reduction, and cell-type annotation, was conducted using established scRNA-seq analysis pipelines. Epithelial cells and malignant epithelial cell populations were identified based on canonical marker expression. RCC2 expressions were quantified using normalized scRNA-seq expression values derived from the Seurat object. Epithelial cells were analyzed under two complementary conditions: (i) malignant epithelial cells only, and (ii) all epithelial cells, including both malignant and non-malignant populations, with adjacent non-tumor tissues included for comparison.

For each analytical setting, RCC2 expression distributions across tissue groups were visualized using violin plots with embedded boxplots. Statistical comparisons between groups were performed using the Wilcoxon rank-sum test.

Human Cell Culture and Animal Housing

Human gastric cancer cell lines and the normal human gastric epithelial cell line GES-1 were obtained from the Cell Bank of the Chinese Academy of Sciences (Beijing, China). Cells were cultured in RPMI-1640 medium (Gibco, USA) supplemented with 10% heat-inactivated fetal bovine serum (FBS) and 1% penicillin–streptomycin solution. All cell lines were maintained at 37 °C in a humidified incubator with 5% CO_2. Cell morphology was routinely monitored, and cultures were regularly tested for contamination. Cells were passaged approximately every 48 h to maintain exponential growth.

All animal experiments were conducted in strict accordance with the guidelines of the Institutional Animal Care and Use Committee (IACUC) of Zhejiang Cancer Hospital (approval number: 2024-12-011). Male 615 mice aged six weeks were used in this study. Animals were acclimatized for one week prior to experimental procedures and maintained under specific pathogen-free (SPF) conditions. Mice were housed in individually ventilated cages under controlled environmental conditions, including a temperature of 22 ± 2 °C, relative humidity of 50 ± 10%, and a 12-h light/dark cycle. Standard laboratory chow and sterile water were provided ad libitum throughout the study.

Sex as a biological variable

Our clinical transcriptomic analyses, including TCGA datasets and patient cohorts from Zhejiang Cancer Hospital, examined both male and female patients, as gastric cancer is a disease affecting both sexes. For *in vivo* animal experiments, our study exclusively examined male mice to minimize phenotypic variability and maintain consistency with established baseline models. Given that the fundamental EPHA3–RCC2–YBX1–ITGB1 signaling axis was identified and validated across mixed-sex human cell lines and patient tissues, the core mechanistic findings are expected to be

relevant for both sexes. However, it is unknown whether the magnitude of *in vivo* tumor growth and peritoneal dissemination exhibits sex-dimorphic effects in female mice.

Lentiviral transduction and plasmid construction

To establish stable knockdown cell lines, short hairpin RNA (shRNA) sequences specifically targeting human *RCC2* and a non-targeting control shRNA (vehicle) were cloned into lentiviral vectors. The specific targeting sequences were as follows: shRCC2-1#, 5'-ATGAACTTCCCATCTGAGTTG-3'; and shRCC2-2#, 5'-AACACAGAACAAGAGATGCGC-3'. RCC2 overexpression and ITGB1 overexpression constructs were generated using standard molecular cloning techniques. All lentiviral vectors were constructed and packaged by GeneChem (Shanghai, China). Lentiviral transduction was performed according to the manufacturer's instructions, followed by antibiotic selection to establish stable cell lines. Plasmids encoding wild-type YBX1 and phosphorylation-deficient mutants (Y162A, Y208A, Y158A, S165A, S174A, and S176A) were generated by site-directed mutagenesis and verified by DNA sequencing. All mutant plasmids were constructed by GeneChem (Shanghai, China).

Western blot analysis

Cells were lysed in RIPA buffer (Beyotime, Cat. No. P0013B) supplemented with protease and phosphatase inhibitors and incubated on ice for 30 min with gentle agitation. Lysates were clarified by centrifugation at 12,000 × g for 15 min at 4 °C, and the supernatants were collected for protein quantification using a BCA protein assay kit. Equal amounts of protein (20–40 μg) were mixed with loading buffer, denatured, and separated by 10% SDS–PAGE, followed by transfer onto PVDF membranes. Membranes were blocked with 5% non-fat milk in TBST for 1 h at room temperature and then incubated overnight at 4 °C with primary antibodies against RCC2 (Abcam, cat. no. ab70788), ITGB1 (Proteintech, cat. no. 12594-1-AP), FAK (Proteintech, cat. no. 12636-1-AP), phosphorylated FAK (p-FAK; Proteintech, cat. no. 83933-1-RR), EPHA3 (Abcam, Cat. No. ab281926), Tubulin (Proteintech, cat. no. 11224-1-AP), Lamin A/C (Proteintech, cat. no. 10298-1-AP), and GAPDH (Proteintech, cat. no. 10494-1-AP). After washing with TBST, membranes were incubated with horseradish

peroxidase (HRP)-conjugated secondary antibodies (1:5000 dilution) for 1 h at room temperature. Protein bands were visualized using an enhanced chemiluminescence (ECL) detection system and captured with a ChemiDoc imaging system (Bio-Rad, USA). Band intensities were quantified using ImageJ software.

Cell proliferation and colony formation assays

Cell proliferation was assessed using the Cell Counting Kit-8 (CCK-8, Cat. No. C0037) assay. Briefly, 3,000 cells were seeded into each well of 96-well plates. At the indicated time points (0 h, 12 h, and 24 h), 10 μL of CCK-8 reagent was added to each well, followed by incubation for 2 h at 37 °C in a humidified incubator with 5% CO_2. Absorbance was measured at 450 nm using a microplate reader (BioTek Instruments, USA). For colony formation assays, cells were seeded at low density in six-well plates and cultured for 10–14 days. Colonies were then fixed, stained, and counted.

Wound healing assay

Cell migration was assessed using a wound-healing assay. NUGC3 and AGS cells were seeded in six-well plates and grown to approximately 90% confluence. A linear scratch was generated using a sterile 200-μL pipette tip, and detached cells were removed by washing with phosphate-buffered saline (PBS). Cells were subsequently maintained in serum-free medium. Images were captured at 0 h and after 48 h using an inverted microscope. Wound closure was quantified by measuring gap widths and calculated using ImageJ software. All experiments were performed in triplicate and repeated independently at least three times.

Transwell migration and invasion assays

Cell migration and invasion were evaluated using Transwell chambers with 8-μm pore size membranes (Corning, USA). For migration assays, 5×10^4 cells suspended in 200 μL serum-free medium were seeded into the upper chamber, while 600 μL medium containing 10% FBS was added to the lower chamber. For invasion assays, the upper membranes were precoated with Matrigel (BD Biosciences, USA) diluted 1:8 in serum-free medium, and 8×10^4 cells were seeded per insert. After incubation for 48 h at 37 °C with 5% CO_2, non-migrated or non-invaded cells were removed, and cells on the lower

surface were fixed with 4% paraformaldehyde and stained with 0.1% crystal violet. Migrated or invaded cells were counted in five randomly selected fields under an inverted microscope.

Rt-qPCR analysis

Total RNA was isolated from cells using TRIzol reagent (Invitrogen, USA) according to the manufacturer's instructions. cDNA synthesis was performed using the PrimeScript™ RT reagent Kit (Takara, Japan). The quantitative PCR was conducted using SYBR Green PCR Master Mix (Roche, Switzerland) on a QuantStudio 5 Real-Time PCR System (Thermo Fisher Scientific, USA). RCC2 mRNA expression was normalized to GAPDH and calculated using the 2^−ΔΔCt method. Primers for RCC2 and GAPDH were designed as follows:

RCC2 Forward: 5’- CTTGGCTCTTCTCACCCCAG-3’

RCC2 Reverse: 5’-GGGAAGGCATTCAGGTGGAA-3’

GAPDH Forward: 5’- ACACCCACTCCTCCACCTTTG-3’

GAPDH Reverse: 5’- TCCACCACCCTGTTGCTGTAG-3’

In vivo tumor models

All animal experiments were approved by the Institutional Animal Care and Use Committee and conducted in accordance with institutional guidelines. For the subcutaneous xenograft model, gastric cancer cells were resuspended in sterile phosphate-buffered saline and injected subcutaneously into the flanks of immunodeficient mice at a density of 5×10^6 cells per mouse. Tumor growth was monitored by measuring tumor length and width with calipers at regular intervals, and tumor volume was calculated using the formula: volume = (length × width^2)/2. At the experimental endpoint, mice were sacrificed, and subcutaneous tumors were excised and weighed.

For the orthotopic gastric cancer model, subcutaneous tumors established as described above were harvested under sterile conditions and cut into small tumor fragments. These tumor blocks were then surgically implanted into the gastric wall of recipient mice to generate orthotopic tumors. Tumor progression was monitored

longitudinally by bioluminescence imaging using luciferase-labeled cells. At the endpoint, stomachs were resected for further analyses, including tumor measurement and histological examination.

For the peritoneal dissemination model, gastric cancer cells were injected intraperitoneally at a density of 5×10^6 cells per mouse. Intraperitoneal tumor burden and dissemination were monitored by bioluminescence imaging. At sacrifice, the peritoneal cavity was carefully examined, and metastatic nodules on peritoneal surfaces and intestinal serosa were recorded and collected for subsequent analyses.

Immunohistochemistry and H&E staining

Tumor tissues were fixed in formalin, embedded in paraffin, and sectioned at 4-μm thickness. For immunohistochemistry (IHC), sections were deparaffinized in xylene and rehydrated through graded ethanol. Endogenous peroxidase activity was blocked with 3% hydrogen peroxide, followed by antigen retrieval in citrate buffer (pH 6.0). After blocking with 5% bovine serum albumin, sections were incubated overnight at 4 °C with primary antibodies against RCC2 or ITGB1. Slides were then incubated with HRP-conjugated secondary antibodies, and immunoreactivity was visualized using 3,3'-diaminobenzidine (DAB). Nuclei were counterstained with hematoxylin, and images were captured using a light microscope (Leica, Germany). Hematoxylin and eosin (H&E) staining was performed on paraffin-embedded sections following standard procedures to assess tissue morphology.

Quantitative proteomic analysis

Quantitative proteomic analysis was performed in control and shRNA-mediated RCC2-knockdown AGS and NUGC3 cells. Total cellular proteins were extracted and processed for LC–MS/MS analysis as described above. Mass spectrometry data were acquired using a data-dependent acquisition (DDA) strategy, and raw data were processed using MaxQuant software. Label-free quantification (LFQ) was applied to determine relative protein abundance across samples. Differentially expressed proteins were identified based on fold-change thresholds ($FC > 1.5$ or $FC < -1.5$) and statistical significance ($P < 0.05$). Proteins meeting the predefined criteria were subjected to

downstream analyses. Venn diagram analysis was performed to identify shared upregulated and downregulated proteins between AGS and NUGC3 cells following RCC2 knockdown. Functional enrichment analyses, including Gene Ontology (GO), Kyoto Encyclopedia of Genes and Genomes (KEGG), and gene set enrichment analysis (GSEA), were conducted to assess the biological processes and signaling pathways associated with RCC2-regulated proteins.

DNA pull-down and mass spectrometry

DNA pull-down assays were performed to identify transcription factors potentially binding to the ITGB1 promoter. Biotin-labeled double-stranded DNA probes corresponding to the ITGB1 promoter region and control probes were synthesized and incubated with nuclear extracts from gastric cancer cells. DNA–protein complexes were captured using streptavidin-coated beads and extensively washed to remove non-specifically bound proteins. Bound proteins were eluted, separated by SDS–PAGE, and visualized by silver staining. Protein bands were subsequently subjected to in-gel digestion and analyzed by LC–MS/MS. Identified proteins were intersected with transcription factor annotations obtained from public databases to generate a list of candidate ITGB1-associated transcription factors for further validation.

Chromatin immunoprecipitation and luciferase reporter assays

Chromatin immunoprecipitation (ChIP) assays were performed to evaluate the binding of YBX1 to the ITGB1 promoter in gastric cancer cells. Briefly, cells were crosslinked with formaldehyde, lysed, and chromatin was fragmented by sonication. Immunoprecipitation was carried out using an anti-YBX1 antibody, with normal IgG serving as a negative control. Following reversal of crosslinks, immunoprecipitated DNA was purified and analyzed by quantitative PCR (qPCR) to assess enrichment of ITGB1 promoter regions.

To comprehensively cover the ITGB1 promoter, three primer pairs targeting proximal, middle, and distal regions spanning from 0 to −2000 bp relative to the transcription start site were designed for ChIP–qPCR analysis. The primer sequences were as follows: Primer-1# (proximal): Forward (TAGCTAGTGCCTCCACCAGT),

Reverse (AGAATTGGCCCAGTCTCAGC); Primer-2# (middle): Forward (CAGGATAGCAGCTTGCCAGT), Reverse (GGAGATTGGGGCTGGAAACA); Primer-3# (distal): Forward (CGAAACGGGACATCAGTGGA), Reverse (CCTCAGTTTCCTCCTCTGCG)

For luciferase reporter assays, DNA fragments containing the wild-type ITGB1 promoter or truncated promoter regions were cloned into luciferase reporter vectors. These reporter constructs were co-transfected with YBX1 expression plasmids into gastric cancer cells. Luciferase activity was measured using a dual-luciferase reporter assay system according to the manufacturer's instructions, and relative promoter activity was normalized to internal control signals. All plasmid constructs were generated by GeneChem (Shanghai, China).

Immunofluorescence (IF) Staining

Immunofluorescence staining was performed to visualize the subcellular localization of YBX1 in gastric cancer cells. Briefly, cells were seeded onto glass coverslips placed in 24-well plates and allowed to adhere overnight. The cells were then fixed with 4% paraformaldehyde for 15 minutes at room temperature, permeabilized with 0.1% Triton X-100 for 10 minutes, and subsequently blocked with 5% bovine serum albumin (BSA) for 30 minutes to prevent nonspecific binding. After blocking, samples were incubated overnight at 4°C with the primary antibody against YBX1 (dilution 1:200) diluted in blocking buffer. The following day, the cells were washed three times with PBS and incubated for 1 hour at room temperature with a fluorophore-conjugated secondary antibody (Alexa Fluor 488 or 594, Invitrogen, USA). Nuclei were counterstained with DAPI (1 μg/mL) for 5 minutes. Finally, coverslips were mounted using anti-fade mounting medium, and fluorescence images were acquired with a laser scanning confocal microscope (Leica Microsystems, Germany) under identical settings.

Nuclear–Cytoplasmic Fractionation

Nuclear and cytoplasmic protein fractions were isolated using the Nuclear and Cytoplasmic Protein Extraction Kit (Beyotime, Cat. No. P0027) following the manufacturer's instructions. Briefly, gastric cancer cells were harvested at

approximately 80–90% confluence, washed twice with ice-cold PBS, and resuspended in Cytoplasmic Extraction Reagent I to gently lyse the plasma membrane. After incubation on ice for 10 minutes, Cytoplasmic Extraction Reagent II was added, and the samples were centrifuged at 16,000 × g for 5 minutes at 4°C to separate the cytoplasmic supernatant. The remaining pellet was then resuspended in Nuclear Extraction Reagent, vortexed intermittently, and incubated for 40 minutes on ice to extract nuclear proteins. Both fractions were collected and quantified using the BCA Protein Assay Kit (Thermo Fisher Scientific). The distribution of YBX1 between nuclear and cytoplasmic compartments was analyzed by Western blotting, with Lamin B1 and Tubulin serving as nuclear and cytoplasmic markers, respectively.

Pharmacological inhibition and nuclear–cytoplasmic fractionation

For kinase inhibitor assays, NUGC3 and AGS cells were seeded into six-well plates and cultured until they reached approximately 70-80% confluence. Cells were then treated with the pan-EPH inhibitor ALW-II-41-27 (0, 0.5, or 1.0 μM, TargetMol, cat no. T4344) or the TRK inhibitor Entrectinib (0, 50, or 100 nM, TargetMol, cat no. T3678) for 4 h. Following the inhibitor treatment, cells were harvested, and nuclear and cytoplasmic protein fractions were isolated as above scribed. Equal amounts of nuclear extracts were resolved by SDS-PAGE and subjected to Western blot analysis. Lamin A/C served as the endogenous nuclear loading control.

Co-immunoprecipitation (Co-IP)

To evaluate endogenous protein–protein interactions, NUGC3 and AGS cells were washed with ice-cold PBS and lysed in moderate RIPA buffer supplemented with protease and phosphatase inhibitor cocktails (Beyotime, Cat. No. P1048). Co-immunoprecipitation assays were performed using a commercial Co-IP kit (Yamei, Cat. No. YJ201) according to the manufacturer's protocol. Briefly, to prevent the co-elution of antibody fragments during downstream analysis, specific primary antibodies were first bound to Protein A/G magnetic beads (Pierce, Thermo Fisher Scientific, USA) and covalently cross-linked using the bis(sulfosuccinimidyl)suberate (BS3) crosslinker (Thermo Fisher Scientific, Cat. No. 21580). Cell lysates were clarified by centrifugation,

and approximately 10% of the total cell lysate was reserved as the input control. The remaining lysates were then incubated with the antibody-crosslinked magnetic beads overnight at 4 °C with gentle rotation. Subsequently, the beads were washed three times with ice-cold lysis buffer to remove non-specific binding. The immunoprecipitated complexes were eluted by boiling in 5× SDS loading buffer at 95 °C for 5 min and analyzed by Western blotting using antibodies against RCC2, YBX1, and EPHA3.

Statistical analysis

All in vitro experiments were performed independently at least three times. Data are presented as mean ± standard deviation (SD). Statistical analyses were conducted using appropriate statistical methods as indicated in the figure legends. Comparisons between two groups were performed using Student's *t* test or Wilcoxon rank-sum test, while multiple-group comparisons were analyzed using one-way analysis of variance (ANOVA) when applicable. Survival analyses were conducted using the Kaplan–Meier method with log-rank tests. A two-sided P value < 0.05 was considered statistically significant.

3. Results

3.1 RCC2 is overexpressed in GC tissues and is associated with tumor metastasis and unfavorable prognosis

We downloaded and processed RNA-seq data (STAR workflow) for 33 TCGA tumor projects from the Genomic Data Commons portal (https://portal.gdc.cancer.gov) and extracted TPM-format expression matrices. Pan-cancer analysis showed that RCC2 expression was elevated in most tumor types compared with adjacent non-tumor tissues, including BLCA, BRCA, CESC, CHOL, COAD, ESCA, READ, and STAD (Figure 1A). We further curated the TCGA-STAD cohort and analyzed paired tumor and matched adjacent samples, which demonstrated significantly higher RCC2 expression in GC tissues than in corresponding non-tumor tissues (Figure 1B). To validate these findings in an independent clinical cohort, we collected specimens from 93 GC patients at Zhejiang Cancer Hospital (141 samples in total) and performed single-cell RNA

sequencing on primary tumors, matched adjacent non-tumor tissues, and corresponding metastatic lesions. Across the epithelial compartment, RCC2 exhibited metastasis-associated upregulation. Among malignant epithelial cells, RCC2 expression was higher in metastatic lesions than in primary tumors, supporting enhanced RCC2 activity in metastatic tumor epithelium (Figure 1C). Extending the analysis to all epithelial cells revealed a graded pattern across tissue contexts, with the highest RCC2 expression in metastatic sites, intermediate levels in primary tumors, and the lowest levels in adjacent non-tumor tissues (Figure 1D). Consistently, Western blotting of five freshly collected paired GC and adjacent tissues further confirmed increased RCC2 protein expression in tumors compared with adjacent non-tumor samples (Figure 1E). Finally, survival analysis using the Kaplan–Meier Plotter database indicated that high RCC2 expression was associated with worse overall survival (OS) and first progression (FP) in patients with GC (Figure 1F).

3.2 RCC2 promotes proliferation, migration, and invasion in GC cells.

To select appropriate models for loss- and gain-of-function studies, we first profiled RCC2 protein abundance across a panel of GC cell lines by Western blotting, which revealed heterogeneous RCC2 expression (Figure 2A). To further investigate the functional role of RCC2, we selected AGS cells with relatively high endogenous RCC2 expression and NUGC3 cells with moderate expression for subsequent experiments. Lentiviral transduction of shRNA effectively silenced RCC2 in both NUGC3 and AGS cells, and RCC2 overexpression was also successfully established, as confirmed by Western blot analysis (Figure 2B–C). CCK-8 assays demonstrated that RCC2 knockdown significantly suppressed the growth of NUGC3 and AGS cells, including at 12 h and 24 h time points (Figure 2D), whereas RCC2 overexpression markedly enhanced cell proliferation (Supplementary Figure 1A). Consistently, colony formation assays showed that RCC2 depletion reduced clonogenic capacity, as reflected by decreased colony numbers (Figure 2E), while RCC2 overexpression increased colony formation (Supplementary Figure 1B). Wound-healing assays further indicated that RCC2 silencing impaired the migratory ability of NUGC3 and AGS cells (Figure 2F–

G), whereas RCC2 overexpression promoted migration (Supplementary Figure 1C–D). In line with these observations, Transwell assays revealed that RCC2 knockdown attenuated both migratory and invasive capacities (Figure 2H–I), while RCC2 overexpression enhanced these malignant phenotypes in GC cells (Supplementary Figure 1E–F).

3.3 RCC2 knockdown suppresses tumor growth and metastatic dissemination in vivo

To evaluate the contribution of RCC2 to GC progression and metastasis in vivo, we established subcutaneous xenograft, orthotopic, and peritoneal dissemination models using RCC2-knockdown and control GC cells. In the subcutaneous xenograft model, tumors in the shRCC2 group exhibited markedly reduced growth compared with controls, as reflected by decreased tumor volumes during follow-up (Figure 3A). At the experimental endpoint, excised subcutaneous tumors further confirmed that RCC2 knockdown reduced both tumor size and tumor weight (Figure 3B–C). Consistent findings were observed in the orthotopic GC model. Bioluminescence imaging showed reduced signal intensity in mice implanted with RCC2-knockdown cells (Figure 3D–E). At sacrifice, resected stomachs demonstrated smaller orthotopic tumors with lower tumor mass in the shRCC2 group (Figure 3F–G). Immunohistochemistry of orthotopic tumor sections verified decreased RCC2 expression in tumors following shRNA-mediated knockdown (Figure 3H). In the peritoneal dissemination model, shRNA-mediated RCC2 knockdown similarly attenuated intraperitoneal tumor burden, as indicated by reduced bioluminescence signal intensity (Figure 3I–J). Macroscopic examination at necropsy revealed a marked decrease in the number of metastatic nodules on the peritoneal surfaces and intestinal serosa in the shRCC2 group (Figure 3K–L), which was further corroborated by hematoxylin and eosin staining (Figure 3M).

3.4 Proteomics identifies ITGB1 as a downstream effector of RCC2 and implicates integrin–FAK signaling in GC cells

To explore the molecular programs regulated by RCC2 in GC cells, we performed quantitative proteomic profiling in control (vehicle) and shRNA-mediated RCC2-

knockdown NUGC3 and AGS cells (Figure 4A). Differential expression analysis identified 43 altered proteins in AGS cells, including 24 upregulated and 17 downregulated proteins relative to controls, whereas 158 differentially expressed proteins were detected in NUGC3 cells, with 49 upregulated and 109 downregulated (Figure 4B; Supplementary Figure 2A–C). We intersected the two proteomic datasets using a Venn diagram to identify conserved RCC2-associated alterations, which highlighted ITGB1 as a shared downregulated protein and RPL38 as a shared upregulated protein in both AGS and NUGC3 cells following RCC2 knockdown (Figure 4C). Notably, ITGB1 encodes the predominant β-subunit of the integrin family and mediates cell–cell and cell–extracellular matrix interactions, a process that has been extensively implicated in tumor invasion and metastasis.

To further interpret the functional relevance of RCC2-associated proteomic alterations, we conducted KEGG and Gene Ontology (GO) enrichment analyses. In AGS cells, KEGG analysis showed enrichment of pathways related to ECM–receptor interaction, protein digestion and absorption, relaxin signaling, focal adhesion, choline metabolism in cancer, proteoglycans in cancer, and the PI3K–Akt signaling pathway (Figure 4D). Consistently, GO analysis highlighted terms associated with the integrin α3β1 complex, integrin-mediated signaling, choline transmembrane transporter activity, transforming growth factor-β receptor signaling, and regulation of growth (Figure 4E). In NUGC3 cells, KEGG enrichment indicated involvement of PI3K–Akt signaling, cell cycle, focal adhesion, and metabolic pathways (Supplementary Figure 2D), while GO analysis was enriched for nuclear-transcribed mRNA catabolic processes, DNA unwinding involved in DNA replication, and DNA replication origin binding (Supplementary Figure 2E). Moreover, GSEA further supported an association between RCC2 knockdown and adhesion-related programs: in AGS cells, enriched terms were dominated by cell–matrix adhesion and focal adhesion (Figure 4F), whereas in NUGC3 cells, the dominant signatures were cell–substrate adhesion and focal adhesion (Supplementary Figure 2F–G).

Given the consistent downregulation of ITGB1 in the proteomic datasets and the enrichment of adhesion-related pathways, we next evaluated the relationship between

RCC2 and ITGB1 in clinical transcriptomic data. Analysis of the TCGA-STAD cohort demonstrated a positive correlation between RCC2 and ITGB1 expression ($R = 0.29$, $P < 0.001$) (Figure 4G). We then assessed ITGB1 and its downstream effector phospho-FAK (p-FAK) in GC cells. Western blotting showed that RCC2 knockdown reduced ITGB1 and p-FAK levels in both NUGC3 and AGS cells (Figure 4H–I), whereas RCC2 overexpression increased ITGB1 and p-FAK expression (Figure 4J–K), supporting a model in which RCC2 promotes integrin–FAK signaling in GC cells.

3.5 ITGB1 restoration reverses the anti-tumor effects of RCC2 knockdown in vitro and in vivo

Based on our proteomic profiling and validation results suggesting a potential link between RCC2 and ITGB1, we next investigated whether ITGB1 contributes to RCC2-associated proliferative and metastatic phenotypes in GC cells. To this end, we established ITGB1-overexpressing AGS and NUGC3 cell lines in the context of shRNA-mediated RCC2 knockdown. Western blot analysis confirmed successful ITGB1 overexpression in RCC2-knockdown cells (Figure 5A). We then performed a series of functional rescue assays. CCK-8 assays showed that ITGB1 overexpression significantly restored the proliferative capacity of AGS and NUGC3 cells suppressed by RCC2 knockdown (Figure 5B). Consistently, colony formation assays demonstrated that re-expression of ITGB1 mitigated the reduction in clonogenic growth caused by RCC2 knockdown (Figure 5C). In addition, wound-healing assays indicated that RCC2 knockdown impaired GC cell migration, whereas ITGB1 overexpression partially rescued migratory ability (Figure 5D–E). Transwell migration and invasion assays further corroborated these findings, showing that ITGB1 re-expression reversed the inhibitory effects of RCC2 knockdown on GC cell migration and invasion.

To extend these observations in vivo, we evaluated the impact of ITGB1 restoration in mouse tumor models. In the subcutaneous xenograft model, RCC2 knockdown resulted in progressively reduced tumor growth over time compared with controls, while ITGB1 overexpression restored tumor growth as assessed by tumor volume (Figure 6A–B) and tumor weight at the endpoint (Figure 6C). Similar patterns

were observed in the orthotopic GC model: bioluminescence imaging revealed that RCC2 knockdown reduced tumor signal intensity, whereas ITGB1 overexpression increased the signal (Figure 6D–E). Endpoint analyses of resected stomachs further confirmed corresponding changes in orthotopic tumor size and tumor mass (Figure 6F–G). Immunohistochemistry of orthotopic tumors showed RCC2 and ITGB1 expression patterns across groups (Figure 6H). Moreover, in the peritoneal dissemination model, mice implanted with RCC2-knockdown cells displayed decreased intraperitoneal bioluminescence, whereas ITGB1 overexpression increased signal intensity (Figure 6I–J). Consistently, necropsy revealed concordant differences in the size and number of metastatic nodules on peritoneal surfaces and intestinal serosa among groups (Figure 6K–L). Collectively, these data support that ITGB1 is a key functional mediator downstream of RCC2 that contributes to GC tumor growth and dissemination.

3.6 RCC2 modulates ITGB1 transcription by controlling YBX1 nuclear localization

To further elucidate the mechanism by which RCC2 regulates ITGB1 expression, we first examined whether RCC2 affects ITGB1 at the transcriptional level. RT–qPCR analysis showed that ITGB1 mRNA expression was significantly reduced following RCC2 knockdown (Figure 7A), suggesting that RCC2 may influence ITGB1 transcription. To identify potential transcription factors involved in ITGB1 regulation, a DNA pull-down assay targeting the ITGB1 promoter was performed. Silver staining revealed distinct differences in proteins enriched by the ITGB1 promoter compared with the control probe (Figure 7B). Proteins pulled down by the ITGB1 promoter were subsequently subjected to mass spectrometry analysis and intersected with transcription factors annotated in the GeneCards database (Figure 7C). Ranking based on score and iBAQ percentage highlighted SFPQ, YBX1, and STAT3 as candidate transcription factors (Figure 7D).

Among these candidates, YBX1 drew particular attention. Overexpression of YBX1 in GC cells markedly increased ITGB1 mRNA levels (Figure 7E). In silico analysis using the JASPAR database identified putative YBX1 binding motifs within

the ITGB1 promoter region (Figure 7F), supporting a potential regulatory interaction. This was further validated by chromatin immunoprecipitation followed by qPCR, which demonstrated that anti-YBX1 antibodies, but not control IgG, significantly enriched ITGB1 promoter sequences, indicating direct binding of YBX1 to the ITGB1 promoter (Figure 7G). To functionally map the critical binding region, we generated luciferase reporter constructs harboring either the full-length ITGB1 promoter or its truncated variants: Δfrag1 (+50 to −1300 bp) and Δfrag2 (+50 to −750 bp). Compared to the empty vector, the full-length ITGB1 promoter significantly enhanced luciferase activity. Notably, the Δfrag1 construct exhibited transcriptional activity comparable to that of the full-length promoter, whereas this activation was drastically attenuated in the Δfrag2 construct (Figure 7H). These results robustly indicate that YBX1 directly binds to the ITGB1 promoter to drive its transcription, with the −1300 to −751 bp region serving as the essential regulatory module.

We next investigated whether RCC2 influences ITGB1 expression through modulation of YBX1 activity. Immunofluorescence staining revealed that RCC2 knockdown markedly reduced the nuclear localization of YBX1 (Figure 7I–J). Consistently, nuclear–cytoplasmic fractionation followed by Western blotting demonstrated that RCC2 knockdown increased cytoplasmic YBX1 levels while reducing nuclear YBX1 abundance (Figure 7K). In contrast, RCC2 overexpression resulted in enhanced nuclear accumulation of YBX1 (Figure 7L). Together, these findings suggest that RCC2 regulates ITGB1 expression by promoting the nuclear localization of the transcription factor YBX1.

3.7 RCC2 interacts with YBX1 and promotes its nuclear translocation through Y162 phosphorylation

Given the observed effect of RCC2 on YBX1 nuclear localization, we next hypothesized that this regulation might be mediated by a direct interaction between RCC2 and YBX1. To test this possibility, protein–protein docking analyses were first performed using ZDOCK and HDOCK prediction algorithms, both of which suggested a potential interaction between RCC2 and YBX1 (Figure 8A–B). This interaction was

further validated experimentally by co-immunoprecipitation assays, which showed that anti-RCC2 antibodies precipitated YBX1 protein compared with IgG controls, while reciprocal immunoprecipitation with anti-YBX1 antibodies also pulled down RCC2 (Figure 8C).

Because protein phosphorylation plays a critical role in transcription factor activation and subcellular localization, we next investigated whether RCC2–YBX1 interaction affects YBX1 phosphorylation. Using the PhosphoSitePlus database, several potential phosphorylation sites on YBX1 were identified, including Y162, Y208, Y158, S165, S174, and S176 (Figure 8D). To functionally assess these sites, plasmids encoding wild-type YBX1 and site-specific phosphorylation-deficient mutants were constructed. Western blot analysis revealed that RCC2 overexpression increased the protein abundance of wild-type YBX1 and most mutant forms, with the notable exception of the Y162A-YBX1 mutant (Figure 8E). Consistent with this observation, in GC cells expressing Y162A-YBX1, RCC2 overexpression failed to enhance ITGB1 and phosphorylated FAK (p-FAK) protein levels, in contrast to cells expressing wild-type YBX1 (Figure 8F). Functional assays further supported the importance of Y162 phosphorylation: colony formation assays demonstrated that Y162A-YBX1 was unable to significantly restore the RCC2-induced increase in proliferative capacity (Figure 8G), and Transwell migration and invasion assays yielded similar results, showing that Y162A-YBX1 abolished the pro-migratory and pro-invasive effects associated with RCC2 overexpression (Figure 8H–I).

Since RCC2 lacks intrinsic kinase activity, we hypothesized that it might act as a scaffold to recruit a specific tyrosine kinase responsible for YBX1 Y162 phosphorylation. To identify the upstream kinase, we performed in silico kinase prediction using the PhosphoSitePlus database, which highlighted the EPHA and TRK families as top candidate kinases for the Y162 motif (Table 1). To experimentally validate this, we subjected GC cells to pharmacological inhibition using specific kinase inhibitors. Markedly, treatment with the pan-EPH inhibitor ALW-II-41-27 drastically abrogated the nuclear accumulation of YBX1, whereas the TRK inhibitor exerted no such effect (Figure 8J). To further elucidate the spatial dynamics of this regulatory

complex, Co-IP assays were performed, demonstrating that RCC2 not only interacts with YBX1 but also physically binds to EPHA3 (Figure 8K). Crucially, we observed a direct interaction between YBX1 and EPHA3, and this interaction was substantially diminished following shRNA-mediated RCC2 knockdown (Figure 8L). Taken together, these data robustly indicate that EPHA3 is the bona fide kinase responsible for YBX1 Y162 phosphorylation, and that RCC2 functions as an indispensable scaffold bridging EPHA3 and YBX1 to facilitate this phosphorylation event and subsequent nuclear translocation.

Discussion

Metastatic dissemination remains the major obstacle to improving survival outcomes in gastric cancer (GC). Despite advances in systemic therapies, the molecular drivers that enable GC cells to acquire invasive and metastatic capabilities are still incompletely understood.[15]. In this context, the present study provides new insight into the role of RCC2 in gastric cancer progression and identifies a previously unrecognized signaling axis that links RCC2 to integrin-dependent metastatic behavior[16].

RCC2 has long been recognized as a mitosis-associated protein essential for chromosome segregation and cell-cycle progression[17]. However, increasing evidence suggests that RCC2 exerts functions beyond mitosis, particularly in regulating cell motility and tumor aggressiveness[18]. Our findings extend this emerging concept by demonstrating that RCC2 is not merely a marker of proliferative activity, but an active regulator of metastatic competence in gastric cancer. The preferential enrichment of RCC2 in malignant epithelial cells and metastatic lesions supports the notion that RCC2 contributes to phenotypic traits required for tumor dissemination rather than representing a general housekeeping factor.

A central contribution of this study is the identification of ITGB1 as a functional downstream effector of RCC2. Integrin β1 (ITGB1) is a core member of the integrin superfamily and plays a fundamental role in mediating cell–extracellular matrix interactions[19]. As part of multiple integrin heterodimers, ITGB1 functions as a bidirectional signaling molecule that links the extracellular environment to intracellular

signaling networks, thereby regulating cell adhesion, migration, proliferation, and survival[20-22]. Dysregulation of ITGB1 has been widely implicated in tumor invasion, metastatic dissemination, and poor clinical outcomes across diverse cancer types[23]. In addition to its role in cell adhesion, ITGB1 activates downstream signaling pathways, including focal adhesion kinase (FAK)–dependent signaling, which are critical for tumor cell motility and metastatic competence[24]. Aberrant ITGB1 signaling has also been associated with lymphatic remodeling and enhanced metastatic spread[25]. Despite extensive evidence supporting the pro-metastatic role of ITGB1, the upstream regulatory mechanisms controlling its expression in gastric cancer have remained poorly defined. Our data suggest that RCC2 functions as an upstream regulator of ITGB1, thereby providing a mechanistic link between RCC2 activity and integrin–FAK signaling. This finding places RCC2 within a well-established pro-metastatic framework and helps explain how RCC2 contributes to invasive tumor behavior.

Importantly, our study further reveals that RCC2 regulates ITGB1 at the transcriptional level. DNA pull-down assays and transcription factor screening identified YBX1 as a key regulator of ITGB1 expression. Y-box binding protein 1 (YBX1), also known as YB1, is a highly conserved and multifunctional nucleic acid–binding protein that has been extensively implicated in cancer development and cellular stress responses[26]. Structurally, YBX1 contains an evolutionarily conserved cold shock domain that enables its interaction with both DNA and RNA, thereby allowing it to function as a versatile regulator of gene expression. In cancer cells, YBX1 has been reported to participate in a broad range of biological processes, including cell proliferation, survival under stress, drug resistance, immune evasion, and chromatin remodeling, underscoring its central role in tumor progression[27-33].

A distinctive feature of YBX1 is its dynamic subcellular localization[34]. Under basal conditions, YBX1 is predominantly retained in the cytoplasm, where it regulates mRNA stability, translation, and post-transcriptional processing[35]. Upon specific oncogenic or stress-related stimuli, YBX1 undergoes post-translational modifications—most notably phosphorylation—that facilitate its translocation into the nucleus. Nuclear YBX1 functions as a transcriptional regulator by binding to promoter

regions of target genes and activating transcriptional programs that support malignant phenotypes[36]. For example, phosphorylated YBX1 translocates to the nucleus, where it binds to the PD-L1 promoter and activates its transcription, thereby contributing to tumor immune evasion[37]. However, the upstream mechanisms governing its phosphorylation-dependent nuclear translocation remain incompletely understood, particularly in the context of gastric cancer metastasis. In this study, we provide evidence that RCC2 serves as an important upstream modulator of YBX1 activity. Crucially, because RCC2 lacks intrinsic kinase activity, we sought to identify the direct enzymatic mediator of YBX1 phosphorylation. Through pharmacological screening and interaction assays, we discovered that the receptor tyrosine kinase EPHA3 serves as the bona fide kinase responsible for phosphorylating YBX1 at the Y162 residue. Our data reveal a novel structural paradigm wherein RCC2 acts as an indispensable scaffold protein, physically bridging EPHA3 and YBX1 in the cytoplasm. By assembling this ternary complex, RCC2 facilitates the EPHA3-mediated phosphorylation of YBX1, a modification that is required for efficient nuclear translocation and transcriptional activation of downstream targets such as ITGB1. Disruption of this regulatory event — either by depleting RCC2 to uncouple the complex or by pharmacologically inhibiting EPHA3— abrogates YBX1 nuclear localization and attenuates integrin–FAK signaling, thereby impairing pro-metastatic cellular behaviors.

Conclusion

In summary, this study provides comprehensive evidence that RCC2 is a key driver of gastric cancer progression and metastasis through transcriptional activation of ITGB1 via YBX1. Specifically, we uncover a novel structural paradigm wherein RCC2 acts as a spatial scaffold, recruiting the EPHA3 kinase to directly phosphorylate YBX1 and trigger its nuclear translocation. Our findings not only deepen the understanding of gastric cancer metastatic mechanisms but also highlight the newly identified EPHA3–RCC2–YBX1 signaling axis as a promising therapeutic target for advanced gastric cancer.

Declarations

Abbreviations

GC: Gastric cancer; RCC2: Regulator of chromosome condensation 2; TCGA: The Cancer Genome Atlas; ITGB1: Integrin beta 1; YBX1: Y-box binding protein 1; EPHA3: Receptor tyrosine kinase EPHA3; GEF: Guanine nucleotide exchange factor; MAPK: Mitogen-activated protein kinase; JNK: c-Jun N-terminal kinase; GPX4: Glutathione peroxidase 4; GDC: Genomic Data Commons; TPM: Transcripts per million; STAD: Stomach adenocarcinoma; OS: Overall survival; FP: First progression ; scRNA-seq: Single-cell RNA sequencing; FBS: Fetal bovine serum; SPF: Specific pathogen-free ; shRNA: Short hairpin RNA; FAK: Focal adhesion kinase ; p-FAK: Phosphorylated focal adhesion kinase; GAPDH: Glyceraldehyde-3-phosphate dehydrogenase; HRP: Horseradish peroxidase; ECL: Enhanced chemiluminescence; CCK-8: Cell Counting Kit-8; PBS: Phosphate-buffered saline; RT–qPCR: Quantitative reverse transcription PCR; IHC: Immunohistochemistry; H&E: Hematoxylin and eosin; LC–MS/MS: Liquid chromatography-tandem mass spectrometry; DDA: Data-dependent acquisition; LFQ: Label-free quantification; GO: Gene Ontology; KEGG: Kyoto Encyclopedia of Genes and Genomes; GSEA: Gene set enrichment analysis; ChIP: Chromatin immunoprecipitation; TSS: Transcription start site; IF: Immunofluorescence; BSA: Bovine serum albumin; DAPI: 4',6-diamidino-2-phenylindole; Co-IP: Co-immunoprecipitation; BS3: Bis(sulfosuccinimidyl)suberate; ANOVA: Analysis of variance; ECM: Extracellular matrix; PI3K: Phosphoinositide 3-kinase ; iBAQ: Intensity-based absolute quantification; TRK: Tropomyosin receptor kinase; PD-L1: Programmed death-ligand 1; NGFR: Nerve growth factor receptor

Ethics approval and consent to participate

The study protocol was approved by the Ethics Committee of Zhejiang Cancer Hospital (approval number: IRB-2023-960(IIT)). All patients provided written informed consent. Animal experiments were approved by the Institutional Animal Care and Use Committee (IACUC) of Zhejiang Cancer Hospital (approval number: 2024-12-011). All procedures were conducted in accordance with the Declaration of Helsinki.

Consent for publication

Not applicable.

Availability of data and materials

The datasets used and/or analyzed during the current study are available from the corresponding author on reasonable request.

Competing interests

The authors declare that they have no competing interests.

Funding

This study was supported by the National Natural Science Foundation of China (Grant Nos. 82304946, 82573745, and 82403546); the Natural Science Foundation of Zhejiang Province (Grant Nos. LBD24H290001, LMS25H160006, and ZCLQN25H1602); the "Jianbing and Lingyan + X" Research and Development Program of Zhejiang Province (Grant No. 2025C02059); and the Major Project of Province-Ministry Co-construction of the Medical and Health Science and Technology Plan of Zhejiang Province (Grant No. WKJ-ZJ-2323); the Postdoctoral Scientific Research Start-up Fund of Zhejiang Cancer Hospital (Grant No. BH2025005).

Author contributions

JX, ZX, and CH conceived the study and provided organization, conception, and supervision. QZ, RZ, and CW conducted the experiments. QL, JW, ZW, CZ, ZH, XY, and YZ contributed to study design and data interpretation. JX drafted the manuscript. All authors read and approved the final manuscript.

Acknowledgements

Not applicable.

Authors' information

Not applicable.

References:

1 Duan, Y., Xu, Y., Dou, Y. & Xu, D. Helicobacter pylori and gastric cancer:

mechanisms and new perspectives. *J Hematol Oncol* **18**, 10 (2025). https://doi.org/10.1186/s13045-024-01654-2
2 Sundar, R. *et al.* Gastric cancer. *Lancet (London, England)* **405**, 2087-2102 (2025). https://doi.org/10.1016/s0140-6736(25)00052-2
3 Smyth, E. C., Nilsson, M., Grabsch, H. I., van Grieken, N. C. & Lordick, F. Gastric cancer. *Lancet* **396**, 635-648 (2020). https://doi.org/10.1016/s0140-6736(20)31288-5
4 Wang, W., Xu, B., Zhang, Z., Fang, K. & Chang, X. RCC2 Expression Stimulates ER-Positive Breast Tumorigenesis. *J Oncol* **2020**, 5619462 (2020). https://doi.org/10.1155/2020/5619462
5 Conche, C. *et al.* Combining ferroptosis induction with MDSC blockade renders primary tumours and metastases in liver sensitive to immune checkpoint blockade. *Gut* **72**, 1774-1782 (2023). https://doi.org/10.1136/gutjnl-2022-327909
6 Coccolini, F. *et al.* Neoadjuvant chemotherapy in advanced gastric and esophago-gastric cancer. Meta-analysis of randomized trials. *Int J Surg* **51**, 120-127 (2018). https://doi.org/10.1016/j.ijsu.2018.01.008
7 Zheng, B. *et al.* High Sugar Induced RCC2 Lactylation Drives Breast Cancer Tumorigenicity Through Upregulating MAD2L1. *Adv Sci (Weinh)* **12**, e2415530 (2025). https://doi.org/10.1002/advs.202415530
8 Rosasco-Nitcher, S. E., Lan, W., Khorasanizadeh, S. & Stukenberg, P. T. Centromeric Aurora-B activation requires TD-60, microtubules, and substrate priming phosphorylation. *Science* **319**, 469-472 (2008). https://doi.org/10.1126/science.1148980
9 Papini, D. *et al.* TD-60 links RalA GTPase function to the CPC in mitosis. *Nat Commun* **6**, 7678 (2015). https://doi.org/10.1038/ncomms8678
10 Bruun, J. *et al.* Regulator of Chromosome Condensation 2 Identifies High-Risk Patients within Both Major Phenotypes of Colorectal Cancer. *Clin Cancer Res* **21**, 3759-3770 (2015). https://doi.org/10.1158/1078-0432.Ccr-14-3294
11 Chen, Q., Jiang, P., Jia, B., Liu, Y. & Zhang, Z. RCC2 contributes to tumor invasion and chemoresistance to cisplatin in hepatocellular carcinoma. *Hum Cell* **33**, 709-720 (2020). https://doi.org/10.1007/s13577-020-00353-7
12 Chen, Z. *et al.* RCC2 promotes breast cancer progression through regulation of Wnt signaling and inducing EMT. *J Cancer* **10**, 6837-6847 (2019). https://doi.org/10.7150/jca.36430
13 Humphries, J. D. *et al.* Proteomic analysis of integrin-associated complexes identifies RCC2 as a dual regulator of Rac1 and Arf6. *Sci Signal* **2**, ra51 (2009). https://doi.org/10.1126/scisignal.2000396
14 Wu, Q. *et al.* BRD4 drives esophageal squamous cell carcinoma growth by promoting RCC2 expression. *Oncogene* **41**, 347-360 (2022). https://doi.org/10.1038/s41388-021-02099-4
15 Verstegen, M. H. *et al.* Metastatic pattern in esophageal and gastric cancer: Influenced by site and histology. *World J Gastroenterol* **26**, 6037-6046 (2020). https://doi.org/10.3748/wjg.v26.i39.6037
16 Fang, X., Xu, J., Jin, K. & Qian, J. Combining of immunotherapeutic approaches with chemotherapy for treatment of gastric cancer: Achievements and limitations. *Int*

Immunopharmacol **118**, 110062 (2023). https://doi.org/10.1016/j.intimp.2023.110062
17 Hu, C. *et al.* Inhibition of glutathione peroxidase 4 suppresses gastric cancer peritoneal metastasis via regulation of RCC2 homeostasis. *Redox Biol* **80**, 103519 (2025). https://doi.org/10.1016/j.redox.2025.103519
18 Calderon-Aparicio, A. *et al.* RCC2 Promotes Esophageal Cancer Growth by Regulating Activity and Expression of the Sox2 Transcription Factor. *Mol Cancer Res* **18**, 1660-1674 (2020). https://doi.org/10.1158/1541-7786.Mcr-19-1152
19 Brakebusch, C. & Fässler, R. beta 1 integrin function in vivo: adhesion, migration and more. *Cancer Metastasis Rev* **24**, 403-411 (2005). https://doi.org/10.1007/s10555-005-5132-5
20 Seguin, L., Desgrosellier, J. S., Weis, S. M. & Cheresh, D. A. Integrins and cancer: regulators of cancer stemness, metastasis, and drug resistance. *Trends Cell Biol* **25**, 234-240 (2015). https://doi.org/10.1016/j.tcb.2014.12.006
21 Sun, R. *et al.* ALKBH5 activates FAK signaling through m6A demethylation in ITGB1 mRNA and enhances tumor-associated lymphangiogenesis and lymph node metastasis in ovarian cancer. *Theranostics* **13**, 833-848 (2023). https://doi.org/10.7150/thno.77441
22 Zhu, X. *et al.* ITGB1-mediated molecular landscape and cuproptosis phenotype induced the worse prognosis in diffuse gastric cancer. *Front Oncol* **13**, 1115510 (2023). https://doi.org/10.3389/fonc.2023.1115510
23 Hamidi, H. & Ivaska, J. Every step of the way: integrins in cancer progression and metastasis. *Nat Rev Cancer* **18**, 533-548 (2018). https://doi.org/10.1038/s41568-018-0038-z
24 Urner, S. *et al.* Identification of ILK as a critical regulator of VEGFR3 signalling and lymphatic vascular growth. *Embo j* **38** (2019). https://doi.org/10.15252/embj.201899322
25 Li, H. *et al.* ZIP10 drives osteosarcoma proliferation and chemoresistance through ITGA10-mediated activation of the PI3K/AKT pathway. *J Exp Clin Cancer Res* **40**, 340 (2021). https://doi.org/10.1186/s13046-021-02146-8
26 Kuwano, M., Shibata, T., Watari, K. & Ono, M. Oncogenic Y-box binding protein-1 as an effective therapeutic target in drug-resistant cancer. *Cancer Sci* **110**, 1536-1543 (2019). https://doi.org/10.1111/cas.14006
27 Wang, L. *et al.* Distinct Roles of m(5)C RNA Methyltransferase NSUN2 in Major Gynecologic Cancers. *Front Oncol* **12**, 786266 (2022). https://doi.org/10.3389/fonc.2022.786266
28 Cui, Q. *et al.* YBX1 knockdown induces renal cell carcinoma cell apoptosis via Kindlin-2. *Cell Cycle* **20**, 2413-2427 (2021). https://doi.org/10.1080/15384101.2021.1985771
29 Su, W. *et al.* LINC00857 Interacting with YBX1 to Regulate Apoptosis and Autophagy via MET and Phosphor-AMPKa Signaling. *Mol Ther Nucleic Acids* **22**, 1164-1175 (2020). https://doi.org/10.1016/j.omtn.2020.10.025
30 Lyabin, D. N., Eliseeva, I. A. & Ovchinnikov, L. P. YB-1 protein: functions and regulation. *Wiley Interdiscip Rev RNA* **5**, 95-110 (2014). https://doi.org/10.1002/wrna.1200

31 Lin, Y. *et al.* CTPS1 promotes malignant progression of triple-negative breast cancer with transcriptional activation by YBX1. *J Transl Med* **20**, 17 (2022). https://doi.org/10.1186/s12967-021-03206-5
32 Martin, E. *et al.* CTP synthase 1 deficiency in humans reveals its central role in lymphocyte proliferation. *Nature* **510**, 288-292 (2014). https://doi.org/10.1038/nature13386
33 Chen, Q. *et al.* Circular RNA ACTN4 promotes intrahepatic cholangiocarcinoma progression by recruiting YBX1 to initiate FZD7 transcription. *J Hepatol* **76**, 135-147 (2022). https://doi.org/10.1016/j.jhep.2021.08.027
34 Zhang, N. *et al.* LINC00240 in the 6p22.1 risk locus promotes gastric cancer progression through USP10-mediated DDX21 stabilization. *J Exp Clin Cancer Res* **42**, 89 (2023). https://doi.org/10.1186/s13046-023-02654-9
35 Li, Y. *et al.* Involvement of CXCL17 and GPR35 in Gastric Cancer Initiation and Progression. *Int J Mol Sci* **24** (2022). https://doi.org/10.3390/ijms24010615
36 Lin, C. *et al.* Modulation of YBX1-mediated PANoptosis inhibition by PPM1B and USP10 confers chemoresistance to oxaliplatin in gastric cancer. *Cancer Lett* **587**, 216712 (2024). https://doi.org/10.1016/j.canlet.2024.216712
37 Ru, B. *et al.* TISIDB: an integrated repository portal for tumor-immune system interactions. *Bioinformatics* **35**, 4200-4202 (2019). https://doi.org/10.1093/bioinformatics/btz210

Figure legends

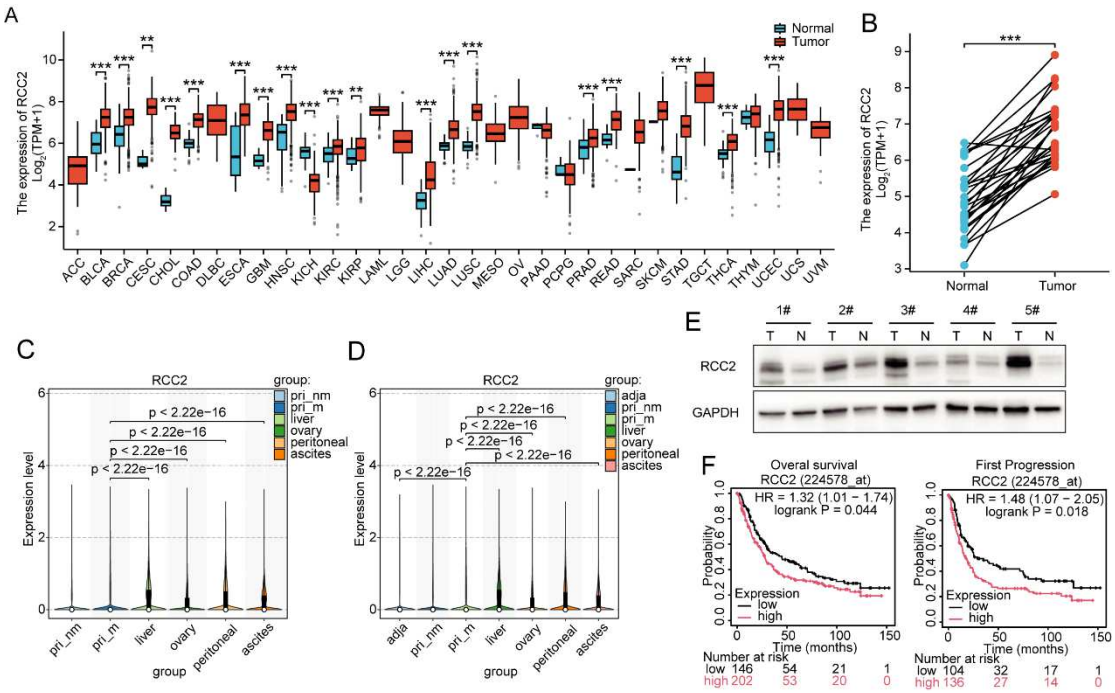


Figure 1. Multi-cohort and multi-omic evaluation of RCC2 expression and clinical relevance in GC. (A) TCGA pan-cancer analysis depicting RCC2 expression in tumor

tissues and adjacent normal tissues. **(B)** RCC2 expression in paired gastric cancer and matched adjacent non-tumor tissues from the TCGA datasets. **(C–D)** Violin plots showing single-cell RNA-seq profiling of RCC2 expression in malignant epithelial cells and in total epithelial cells from the Zhejiang Cancer Hospital cohort. **(E)** Representative Western blot images and densitometric quantification of RCC2 protein levels in five freshly collected paired gastric cancer and adjacent non-tumor tissues. **(F)** Kaplan–Meier Plotter survival curves illustrating overall survival and first progression in gastric cancer patients stratified by RCC2 expression.

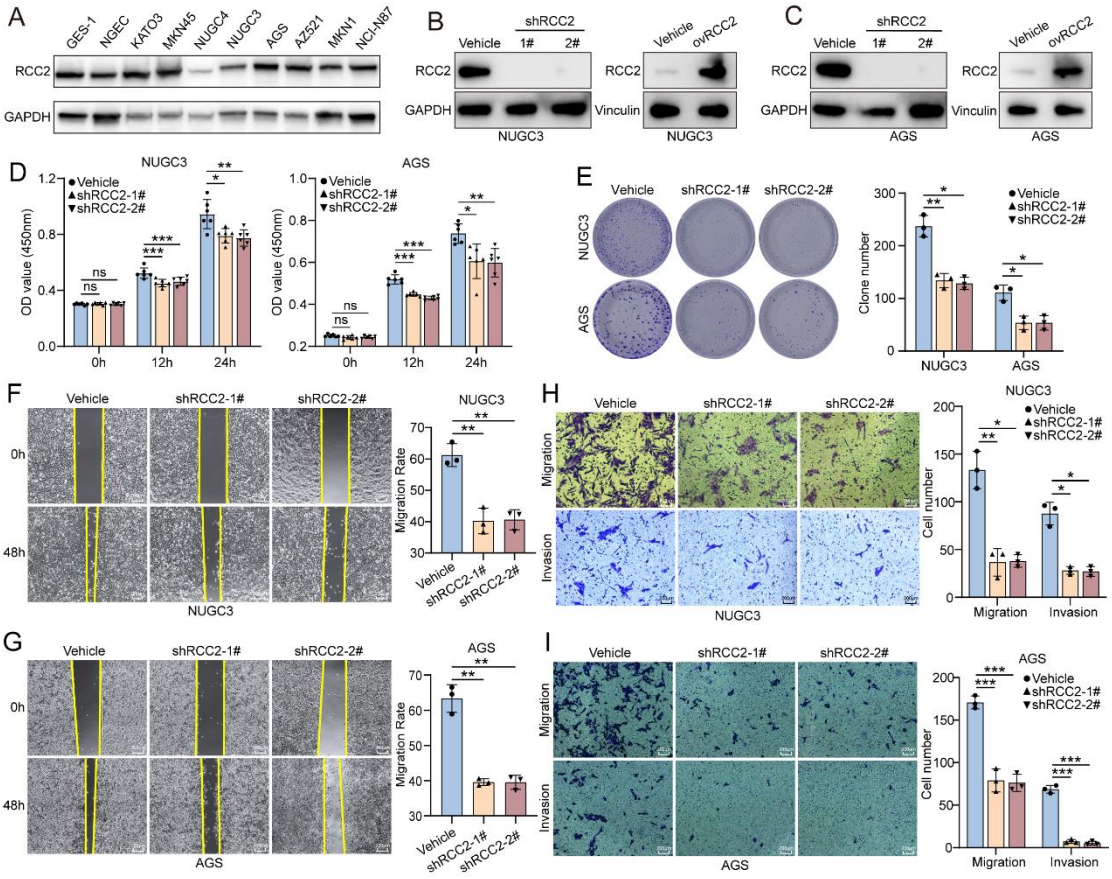


Figure 2. RCC2 loss-of-function inhibits gastric cancer cell proliferation, migration, and invasion. (A) Western blot analysis of RCC2 protein expression across gastric cancer cell lines. **(B–C)** Western blot validation of RCC2 knockdown and RCC2 overexpression in NUGC3 and AGS cells following lentiviral transduction. **(D)** CCK-8 assay assessing cell viability/proliferation in RCC2-silenced NUGC3 and AGS cells. **(E)** Colony formation assay evaluating clonogenic growth in RCC2-silenced NUGC3

and AGS cells. **(F–G)** Wound-healing assays measuring migratory capacity in RCC2-silenced NUGC3 and AGS cells, with representative images and corresponding quantification. **(H–I)** Transwell migration and invasion assays in RCC2-silenced NUGC3 and AGS cells, with representative images and corresponding quantification.

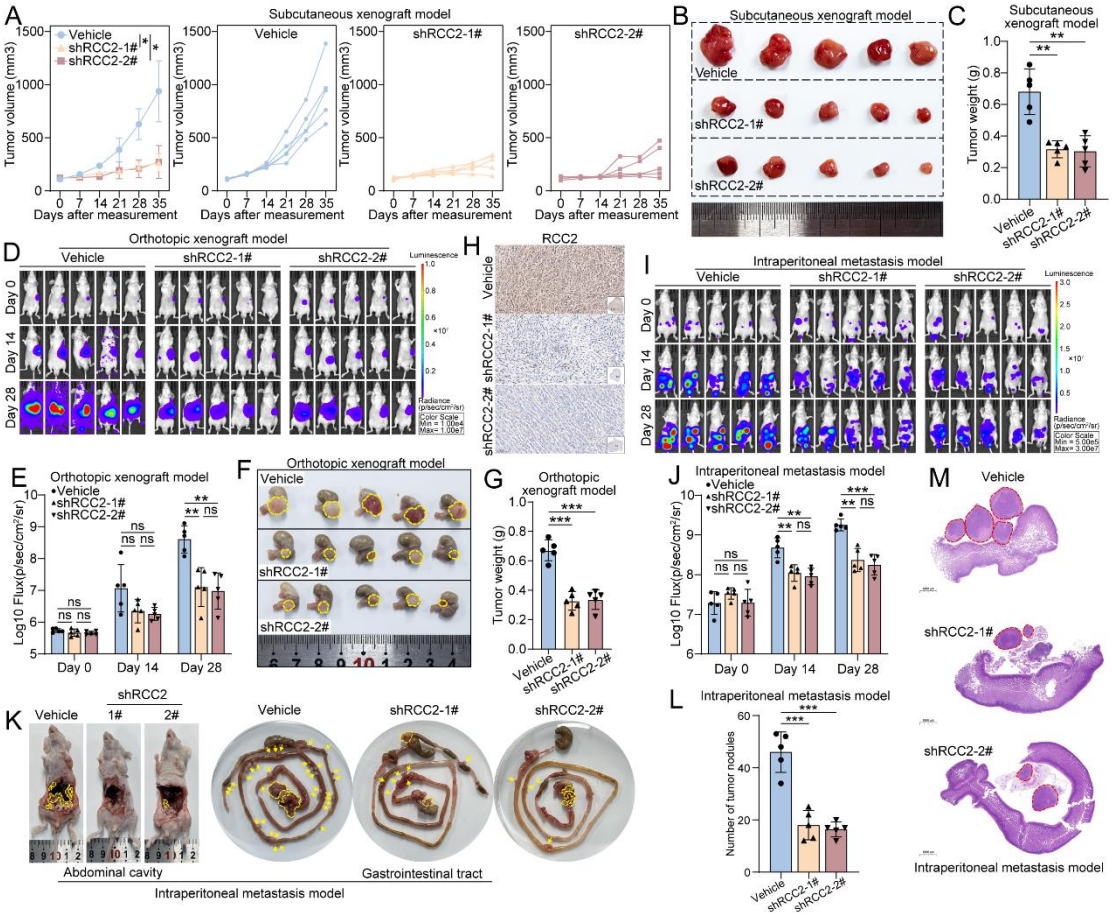


Figure 3. shRNA-mediated RCC2 knockdown inhibits gastric cancer growth and peritoneal dissemination in vivo. (A) Tumor growth curves (tumor volume) of subcutaneous xenografts formed by control and shRCC2 gastric cancer cells. **(B)** Representative images of excised subcutaneous tumors from each group at the experimental endpoint. **(C)** Tumor weights of subcutaneous xenografts at the endpoint. **(D–E)** In vivo bioluminescence imaging of the orthotopic gastric cancer model and corresponding quantification of bioluminescence signal intensity. **(F)** Representative images of resected stomachs showing orthotopic tumors at the endpoint. **(G)** Tumor weights of orthotopic gastric tumors at the endpoint. **(H)** Immunohistochemical staining of RCC2 in orthotopic tumor tissues. **(I–J)** In vivo bioluminescence imaging

of the peritoneal dissemination model and corresponding quantification of bioluminescence signal intensity. **(K)** Representative images of the peritoneal cavity and intestinal surfaces showing metastatic nodules at necropsy. **(L)** Quantification of peritoneal and intestinal metastatic nodules. **(M)** Representative hematoxylin and eosin staining of metastatic lesions from the peritoneal dissemination model.

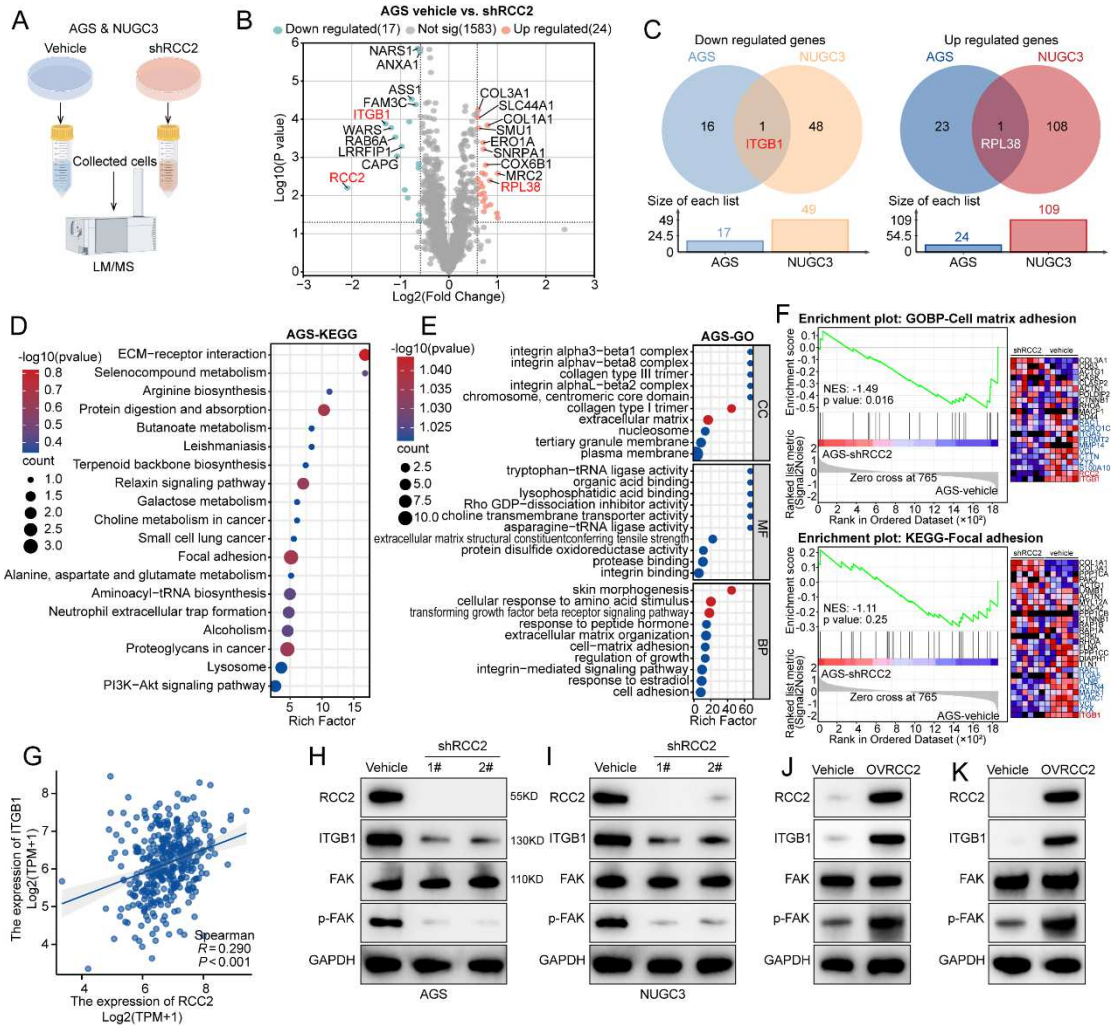


Figure 4. Quantitative proteomics and downstream validation of RCC2-associated signaling in gastric cancer cells. (A) Schematic workflow of the LC–MS/MS-based quantitative proteomic analysis performed in vehicle and shRCC2-treated GC cells. **(B)** Volcano plot of differentially expressed proteins in AGS cells comparing shRCC2 versus control conditions. **(C)** Venn diagram showing the overlap of upregulated and downregulated proteins between AGS and NUGC3 cells after RCC2 knockdown. **(D–E)** KEGG pathway enrichment analysis and GO enrichment analysis of differentially

expressed proteins in AGS cells. **(F)** GSEA plots based on KEGG and GO gene sets in AGS cells. **(G)** Correlation analysis of RCC2 and ITGB1 expression in the TCGA dataset. **(H–I)** Western blot analysis of ITGB1 and p-FAK protein levels in AGS and NUGC3 cells following shRNA-mediated RCC2 knockdown. **(J–K)** Western blot analysis of ITGB1 and p-FAK protein levels in AGS and NUGC3 cells following RCC2 overexpression.

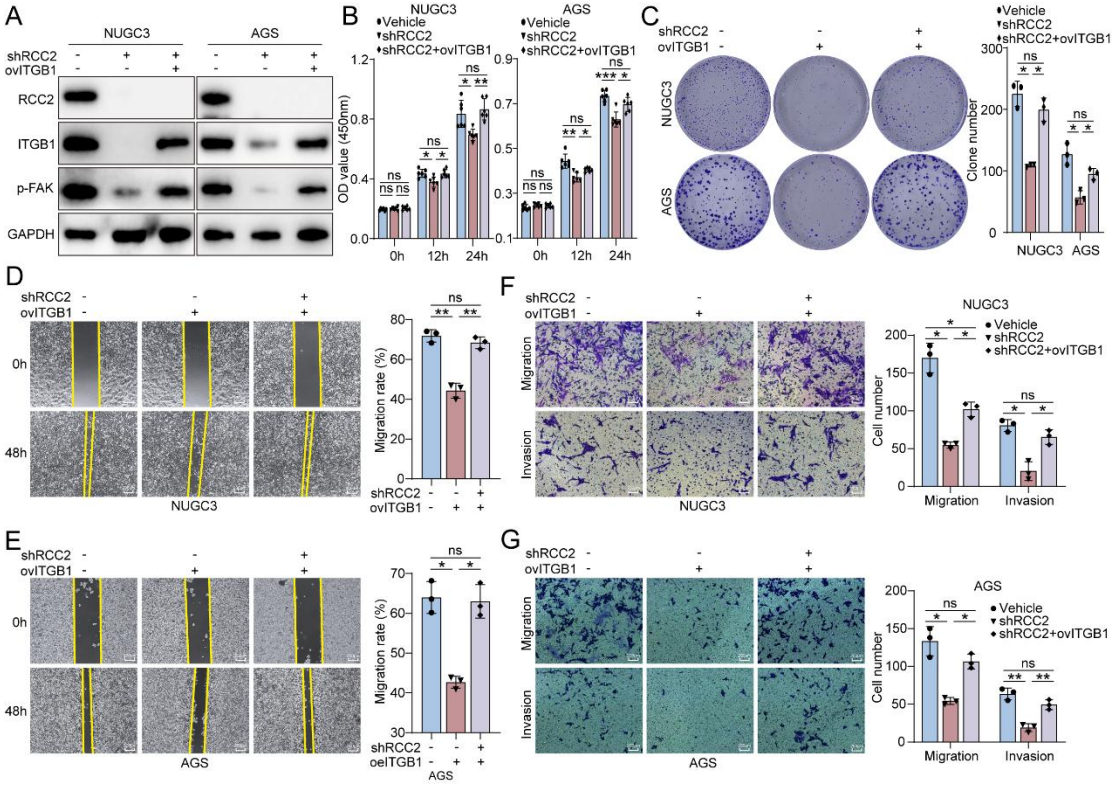


Figure 5. ITGB1 overexpression rescues RCC2 knockdown–induced suppression of malignant phenotypes in gastric cancer cells in vitro. (A) Western blot analysis of ITGB1 protein levels in AGS and NUGC3 cells with shRNA-mediated RCC2 knockdown with or without ITGB1 overexpression. **(B)** CCK-8 assays assessing cell viability/proliferation in AGS and NUGC3 cells across the indicated groups. **(C)** Colony formation assays evaluating clonogenic growth in AGS and NUGC3 cells across the indicated groups. **(D–E)** Wound-healing assays measuring migratory capacity in AGS and NUGC3 cells across the indicated groups, with representative images and corresponding quantification. **(F–G)** Transwell migration and invasion assays in AGS and NUGC3 cells across the indicated groups, with representative

images and corresponding quantification.

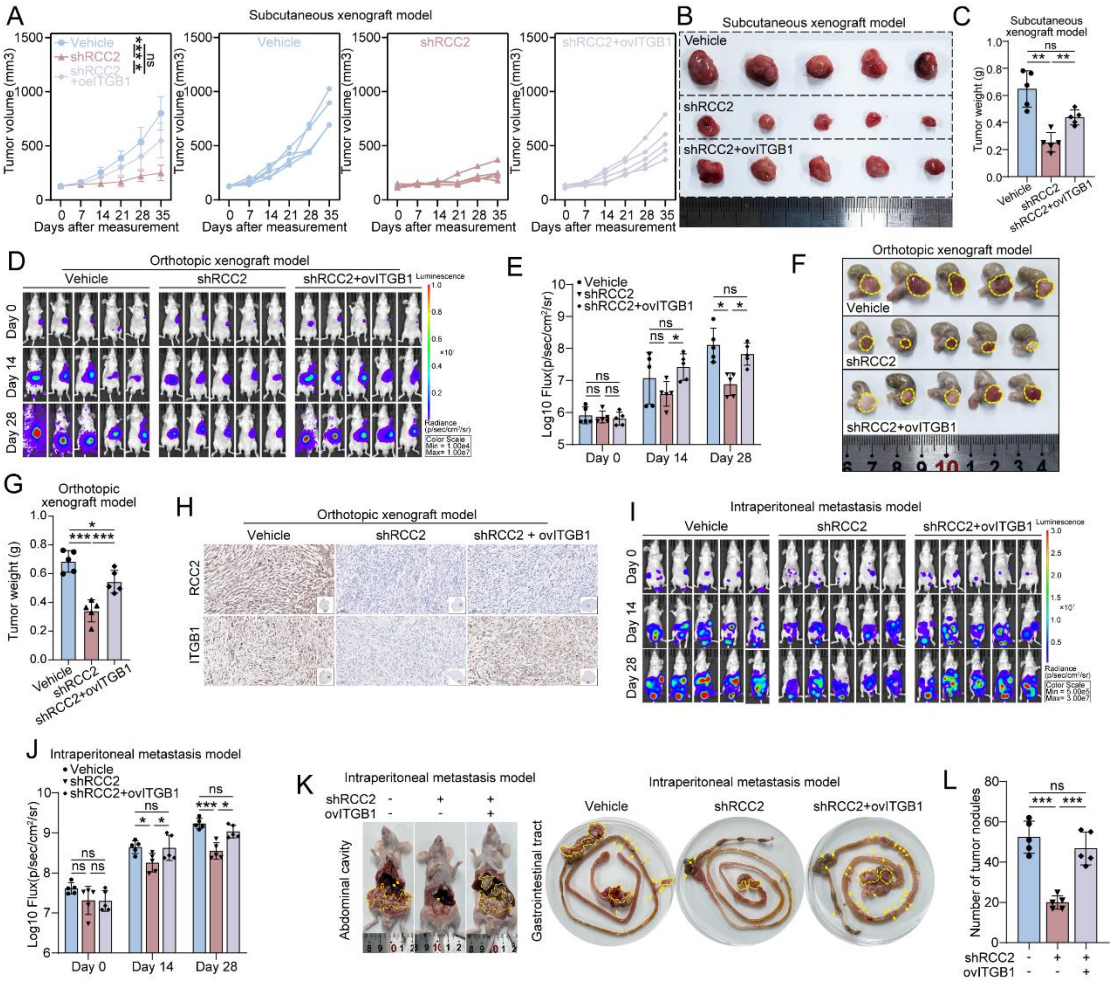


Figure 6. ITGB1 overexpression counteracts the inhibitory effects of RCC2 knockdown on tumor growth and dissemination in vivo. (A–B) Tumor growth curves (tumor volume) and endpoint tumor volume comparison in the subcutaneous xenograft model among the indicated groups. **(C)** Tumor weights of subcutaneous xenografts at the experimental endpoint. **(D–E)** In vivo bioluminescence imaging of the orthotopic gastric cancer model and corresponding quantification of bioluminescence signal intensity among the indicated groups. **(F)** Representative images of resected stomachs showing orthotopic tumors at the endpoint. **(G)** Tumor weights of orthotopic gastric tumors at the endpoint. **(H)** Immunohistochemical staining of RCC2 and ITGB1 in orthotopic tumor tissues from each group. **(I–J)** In vivo bioluminescence imaging of the peritoneal dissemination model and corresponding quantification of bioluminescence signal intensity among the indicated groups. **(K)** Representative

images of the peritoneal cavity and intestinal surfaces showing metastatic nodules at necropsy. **(L)** Quantification of peritoneal and intestinal metastatic nodules among the indicated groups.

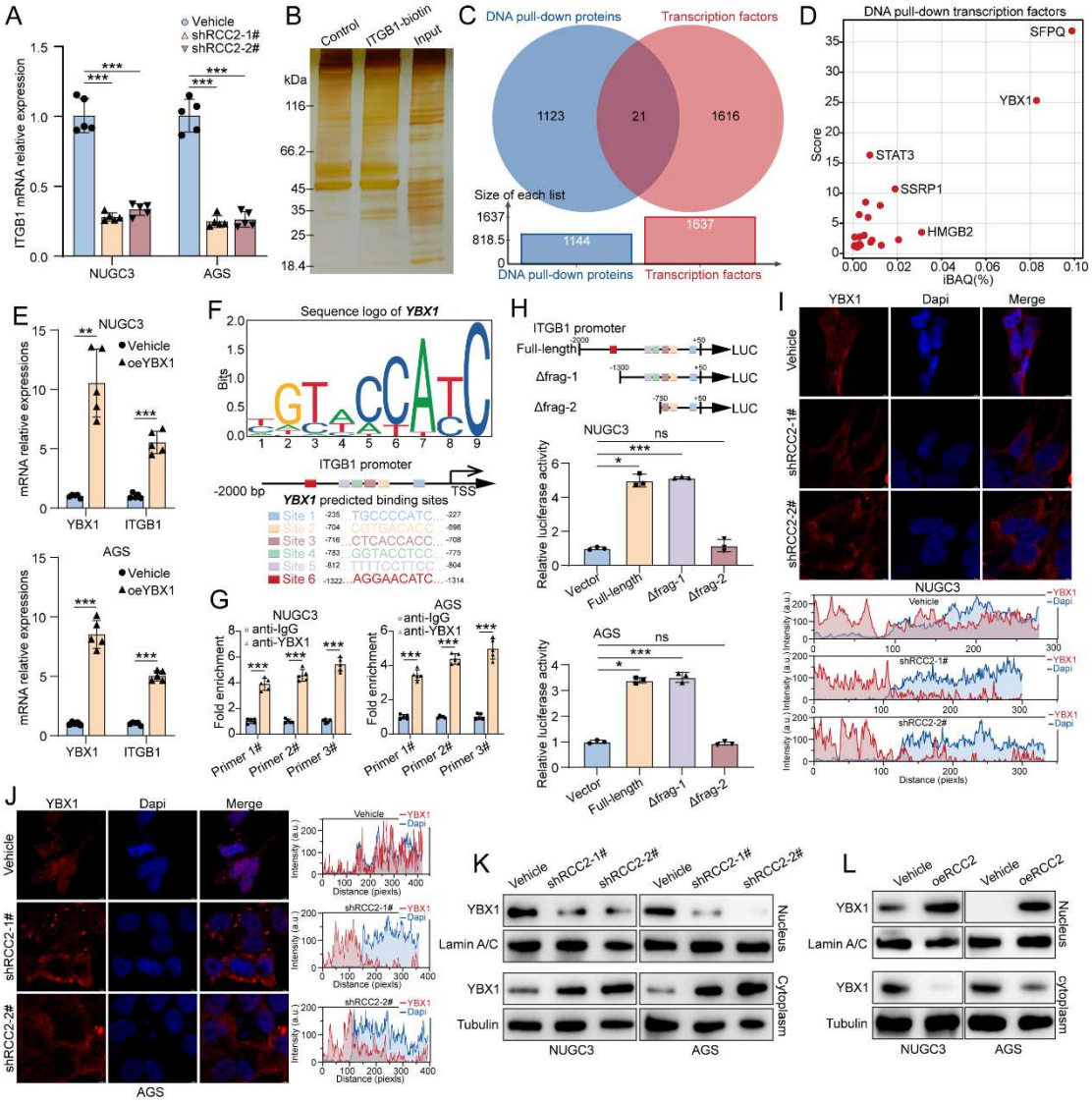


Figure 7. RCC2 regulates ITGB1 transcription through modulation of YBX1 nuclear localization. (A) RT–qPCR analysis of ITGB1 mRNA expression in gastric cancer cells following shRNA-mediated RCC2 knockdown. **(B)** Silver staining of proteins pulled down by the ITGB1 promoter probe and control probe in the DNA pull-down assay. **(C)** Venn diagram showing the intersection between proteins identified by ITGB1 promoter pull-down and transcription factors annotated in the GeneCards database. **(D)** Ranking of candidate transcription factors based on mass spectrometry score and iBAQ percentage. **(E)** RT–qPCR analysis of ITGB1 mRNA expression in

gastric cancer cells following YBX1 overexpression. **(F)** YBX1 sequence logo and predicted YBX1 binding sites within the ITGB1 promoter region identified by JASPAR analysis. **(G)** ChIP–qPCR analysis showing enrichment of ITGB1 promoter fragments immunoprecipitated with anti-YBX1 antibody compared with IgG control. **(H)** Luciferase reporter assays of wild-type and truncated ITGB1 promoter constructs in gastric cancer cells with YBX1 overexpression. **(I–J)** Immunofluorescence staining showing subcellular localization of YBX1 in gastric cancer cells following RCC2 knockdown. **(K)** Western blot analysis of YBX1 protein levels in nuclear and cytoplasmic fractions after RCC2 knockdown. **(L)** Western blot analysis of YBX1 protein levels in nuclear and cytoplasmic fractions after RCC2 overexpression.

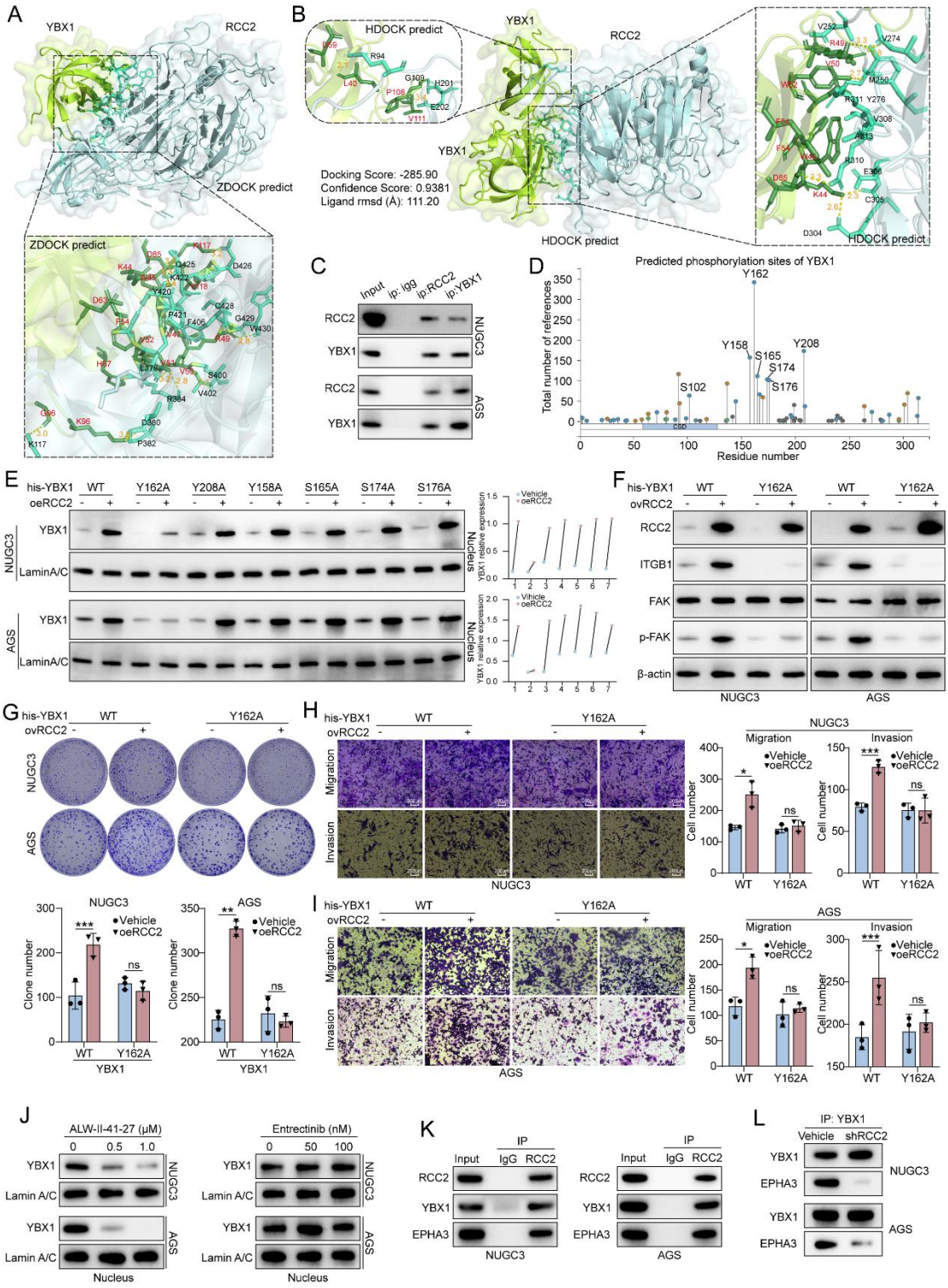


Figure 8. RCC2 interacts with YBX1 and promotes YBX1 Y162-dependent activity. **(A–B)** Protein–protein docking predictions of the RCC2–YBX1 interaction generated using ZDOCK and HDOCK algorithms. **(C)** Co-immunoprecipitation assays showing the interaction between endogenous RCC2 and YBX1, with reciprocal pull-down using anti-RCC2 or anti-YBX1 antibodies and IgG as control. **(D)** Predicted phosphorylation

sites of YBX1 identified using the PhosphoSitePlus database. **(E)** Western blot analysis of YBX1 protein levels in gastric cancer cells expressing wild-type YBX1 or site-specific YBX1 mutants following RCC2 overexpression. **(F)** Western blot analysis of ITGB1 and p-FAK protein expression in gastric cancer cells expressing wild-type YBX1 or the Y162A-YBX1 mutant in the context of RCC2 overexpression. **(G)** Colony formation assays assessing proliferative capacity in gastric cancer cells expressing wild-type YBX1 or Y162A-YBX1 with RCC2 overexpression. **(H–I)** Transwell migration and invasion assays evaluating the migratory and invasive abilities of gastric cancer cells expressing wild-type YBX1 or Y162A-YBX1 with RCC2 overexpression. (J) Western blot analysis of nuclear and cytoplasmic YBX1 protein levels in gastric cancer cells following a 4-hour treatment with the pan-EPH inhibitor ALW-II-41-27 or the TRK inhibitor (K) Co-immunoprecipitation assays demonstrating the endogenous physical interaction among RCC2, YBX1, and the EPHA3 kinase in gastric cancer cells. (L) Co-immunoprecipitation assays evaluating the binding affinity between YBX1 and EPHA3 in GC cells stably expressing vehicle or shRCC2.

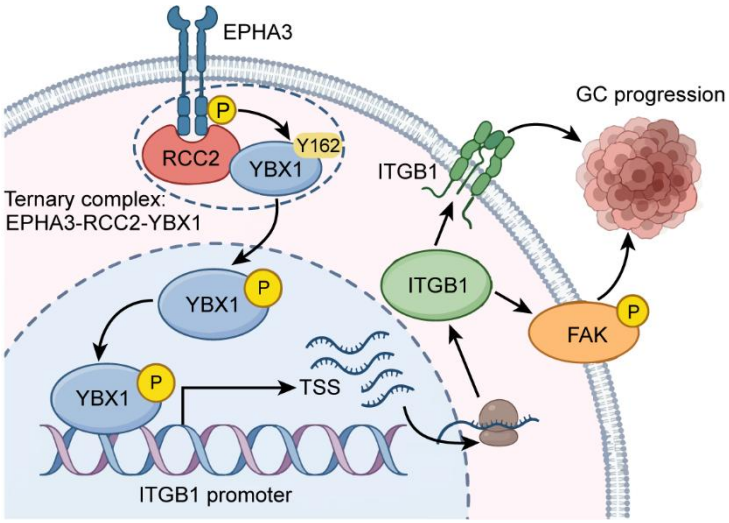
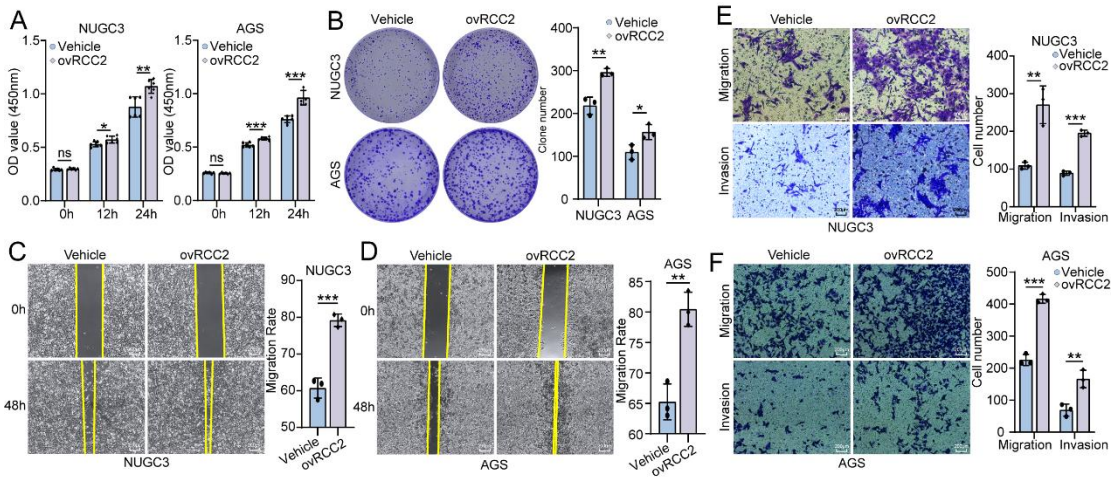
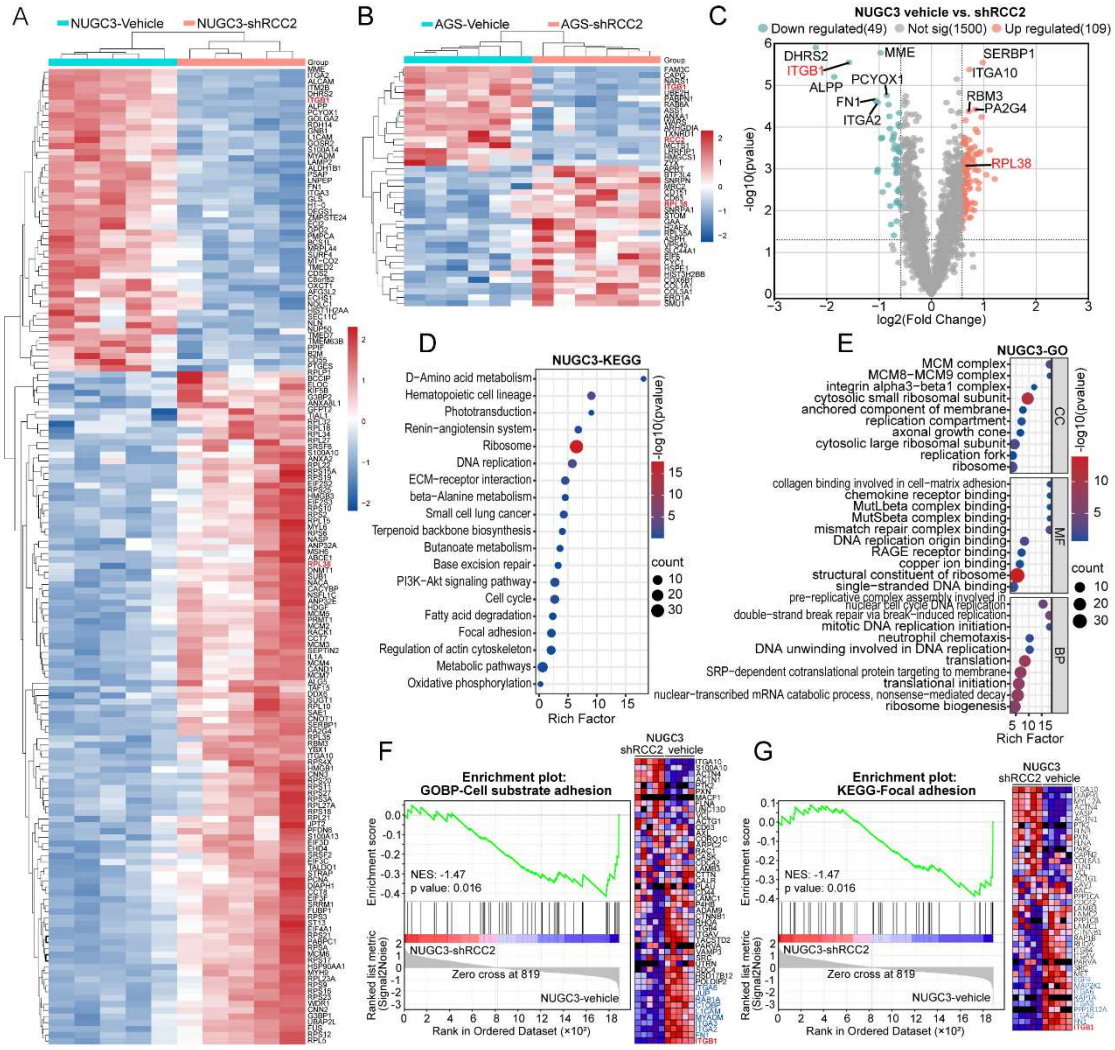


Figure 9. Proposed model illustrating the scaffold-dependent EPHA3–RCC2–YBX1–ITGB1 signaling axis in gastric cancer progression. In gastric cancer cells, RCC2 functions as a crucial spatial scaffold that physically bridges the receptor tyrosine kinase EPHA3 and the transcription factor YBX1, assembling a functional ternary complex. This structural assembly facilitates the EPHA3-mediated phosphorylation of

YBX1 at the Y162 residue. The phosphorylation event triggers YBX1 nuclear translocation, where it directly binds to the ITGB1 promoter to activate its transcription. Subsequently, elevated ITGB1 expression at the cell membrane activates downstream FAK signaling (p-FAK), ultimately driving aggressive malignant phenotypes and gastric cancer progression.



Supplementary Figure 1. RCC2 overexpression enhances gastric cancer cell proliferation, migration, and invasion. **(A)** CCK-8 assay assessing cell viability/proliferation in RCC2-overexpressing gastric cancer cells. **(B)** Colony formation assay evaluating clonogenic growth in RCC2-overexpressing gastric cancer cells. **(C–D)** Wound-healing assays measuring migratory capacity in RCC2-overexpressing gastric cancer cells, with representative images and corresponding quantification. **(E–F)** Transwell migration and invasion assays in RCC2-overexpressing gastric cancer cells, with representative images and corresponding quantification.



Supplementary Figure 2. Proteomic profiling and functional enrichment analyses in NUGC3 cells. (A–B) Heatmaps of differentially expressed proteins in AGS and NUGC3 cells comparing shRCC2 versus control conditions. **(C)** Volcano plot of differentially expressed proteins in NUGC3 cells comparing shRCC2 versus control conditions. **(D–E)** KEGG pathway enrichment analysis and GO enrichment analysis of differentially expressed proteins in NUGC3 cells. **(F–G)** GSEA plots based on KEGG and GO gene sets in NUGC3 cells.

Table 1. Predicted candidate kinases for YBX1 Y162 phosphorylation.

Kinase	Kinase Family	Log_2(Score)	Site Percentile	Percentile Rank
TRKA	NGFR	1.538	93.3	1
EPHA3	EPHR	1.6309	91.46	2
EPHA5	EPHR	2.0852	89.6	3
EPHB3	EPHR	1.8243	88.34	4

TRKC	NGFR	1.359	88.29	5